Department of Precision and Microsystems Engineering

Origami for tunable vibration isolation

R.M. Boere

Report no : 2021.032
Coach : A.M. Aragón
Professor : A. van Keulen
Specialisation : Engineering Mechanics
Type of report : Thesis
Date : 26 May 2021

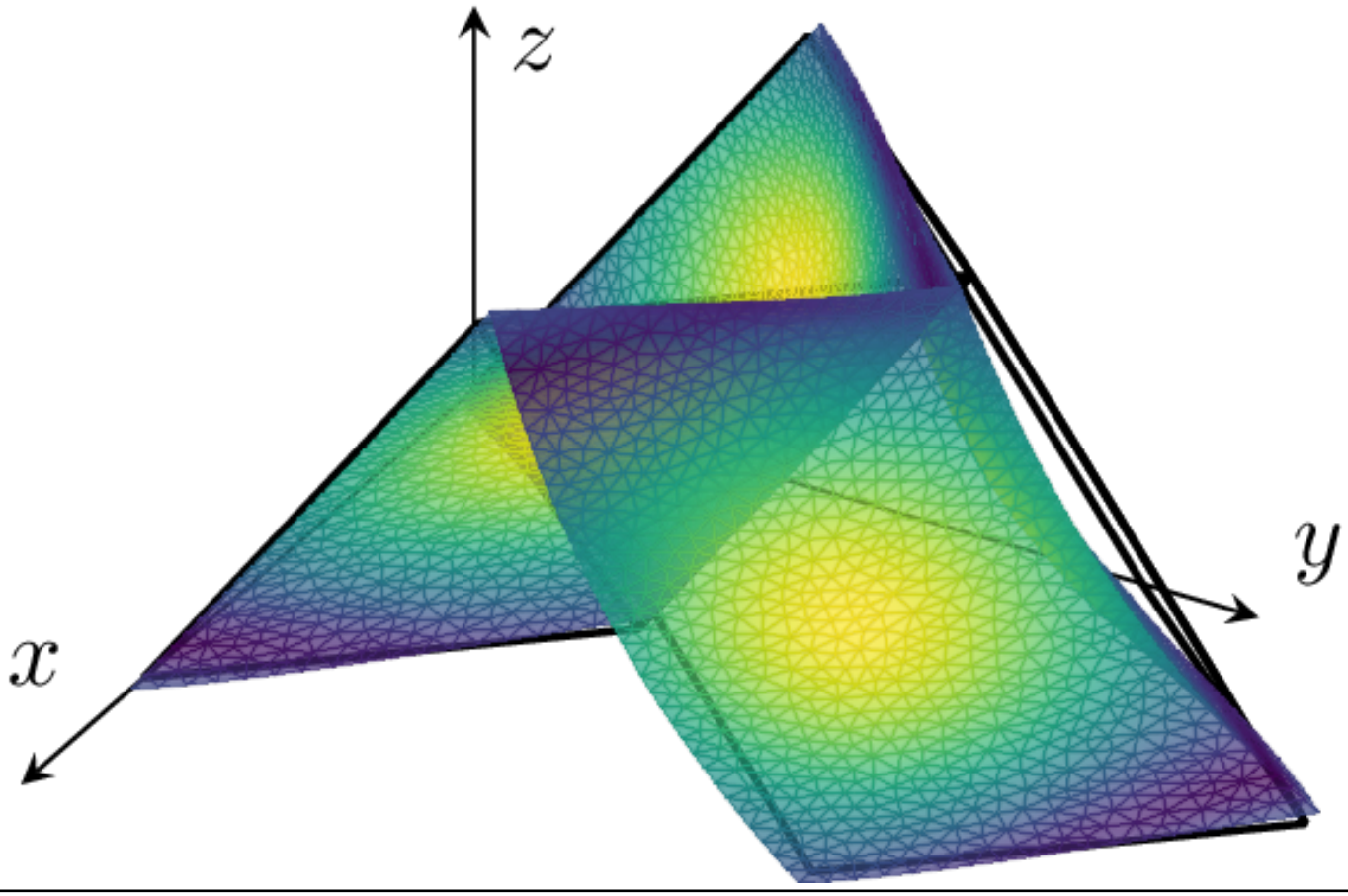

TU Delft Delft University of Technology

Challenge the future

Origami for tunable vibration isolation

by

R.M. Boere

to obtain the degree of Master of Science
at the Delft University of Technology,
to be defended publicly on Wednesday May 26, 2021 at 2:00 PM.

Student number:	4356012	
Project duration:	September 1, 2019 – May 26, 2021	
Thesis committee:	Dr. A. M. Aragón,	TU Delft, supervisor
	Dr. F. Alijani,	TU Delft
	Y. Yan,	TU Delft

TU Delft

Abstract

It is relevant for various applications to seek a material that could be used for the active control of wave propagation. In this study, we explore tunable metamaterials based on foldable origami sheets where the size of the bandgap can be tuned by the rigid folding along predefined crease lines. A combination of out-of-plane components and a crease results in the coupling and separation of bands in the band structure and eventually in a (modal) bandgap. The location, size, and vibration isolation performance are optimized and analyzed for a set of geometrical and material parameters, resulting in a potential design of a Miura-Ori structure. The methods used in this paper could be used for any kind of origami structure, which may lead to various new applications in the field of vibrations and acoustics.

Acknowledgments

Although the thesis is an individual project, I have not done it fully on my own. Without the contribution of some others, the thesis would not be as it is now. I would therefore like to thank some people that have assisted me during the project.

First and foremost my supervisor Alejandro. His enthusiasm and help motivated me a lot to keep making progress. Discussions were always fruitful and helpful, which further motivated me to continue. I am also grateful for his empathy and helpfulness with my personal circumstances.

I would also like to thank my family and friends for the support. Although they do not understand the topics, they were of great help with motivating me.

R.M. Boere
Delft, May 2021

Contents

1 Introduction

The folding of paper originated in Japan and is called origami, which originated from the Japanese words for fold (oru) and paper (kami) [41]. It was previously mostly used for the creation of decorative models, but in recent years it has gained attention from scientists and engineers which try to use the folding of plates for technological applications. This process is sometimes referred to as *Origamics* [79] or *Orimimetrics* [89].

The possibilities of origami seem to be endless, which is for instance reflected in the large number of aesthetic models over the years. Robert J. Lang lists numerous examples of possible origami models in one of his books [38], some of these examples are: elephants, birds, cars and clapping monkeys. Nearly all of these models, which are estimated to be well over the thousands [38], were invented in the last 60 years, many of them using mathematical algorithms or computer programs. Well known software are for example Robert Lang's TreeMaker [62] and Origamizer from Tachi [81].

Also outside the scope of decorative models, there is a rich list of possibilities. Literature studies by Turner et al. [89] and Li et al. [43] list several of these applications, which are for example in packaging, deployable (space) structures, biomedical devices, robotics and architectural structures.

Studies by Pratapa et al. [65] and Nanda and Karami [54] show that origami (foldable plates) could also be used for vibration isolation, acoustic wave guides and noice control applications. By the simple act of folding, a *tunable acoustic metamaterial* could be designed that can block a specific range of frequencies from propagating through the origami sheets, resulting in a band gap.

1.1. Origami

1.1.1. Miura-ori

The most well known and studied origami pattern is the Miura-Ori pattern, named after K. Miura. This pattern was invented for the easy deployment of solar panel arrays in space [53], as this pattern would have one degree of freedom, if folded from an ideal material with infinite stretching modulus [77]. In practice however, this is never the case, so it has some additional degrees of freedom.

The Miura-Ori is flat foldable pattern and has opposite Poisson's ratios for in-plane and out-of-plane deformations. It has negative Poisson's ratio for planar deformations and a positive and equal Poisson's ratio for bending [71]. The negative Poisson's ratio property is not found naturally in nature, which makes the Miura-Ori a metamaterial.

1.1.2. Other patterns

The Miura-Ori pattern is a special type of 4-vertex sheet: a structure composed of cells with four rigid panels connected by four hinges (folds) that meet in one point [94]. The Miura-Ori pattern is a periodic 4-vertex that is flat-foldable and where two crease lines are colinear.

A more general origami sheet could be made by fitting together several 4-vertex unit cells. This was for example done by Dieleman et al. [16]. They showed that there are 140 different types of 4-vertex unit cells, which they represented as jigsaw puzzle pieces. New origami patterns could then be systematically created by combining the pieces into a jigsaw puzzle.

Origami sheets could also be constructing using topology optimization in combination with the ground structure approach [24]. The fold angle is then the design variable, and a fold angle of 0 would mean that

there is no crease at that fold line.

1.1.3. Origami mechanics

Origami models can deform in several ways: by folding along the crease lines, by bending of the panels and by extension or contraction of the panels. In some cases, one or more deformation modes are neglected. For example: in the case of rigid origami, it is assumed that the structure only deforms along the crease lines. The faces between the folds will remain flat. Origami will be considered rigid if the *origami length* [8] $L* = \frac{B}{\kappa}$, the ratio between the bending modulus B of the planes and the torsional stiffness κ of the crease is large compared to the characteristic length of the pattern.

In most papers, the bending of the Miura-Ori facets is modeled by introducing an additional fold line, which is the diagonal of the panels [65, 71, 97]. The panel is then subdivided into two triangular faces that will, according to Demaine et al. [15], remain planar, see Fig. 1.1. They showed that when the boundary of an facet is piecewise linear, the facets will remain piecewise planar when deforming. According to Schenk and Guest [71], the choice of which diagonal to use does not matter for the first order approximation.

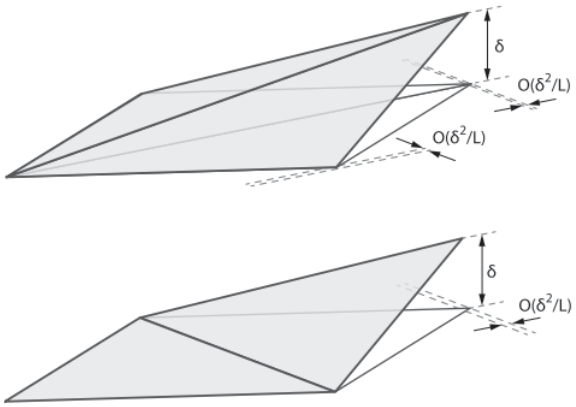

Figure 1.1: Deformation of a facet of the Miura-Ori sheet, along the diagonal bend lines [71].

A study by Filipov et al. [20] shows significant bending behavior of the panels in several of the mode shapes of origami tubes. Which leads to believe that the bending of the panels may have a major influence on the vibration behavior. A study by Nanda and Karami [54] therefore used deformable beams instead of rigid beams. They found that the stiffness ratio between the beams and the fold had an effect on the band structure over which flexural waves propagate. For the 1 dimensional folded sheet they used, the largest band gap was obtained for almost rigid beams and low stiffness folds. The rigid panel assumption is therefore likely the upper limit for the size of the band gap.

For origami panels, Pratapa et al. [65] argue that the panel bending and stretching plays a critical role in the dynamic behavior of origami structures. And they say that the rigid panel assumption is too restrictive. Instead, the origami should be modeled with an alternative description. According to Lebée [41], origami structures could alternatively be modeled as an assembly of shell elements, membrane elements or truss elements.

The crease line is typically modeled as a linear torsional spring with stiffness k_t per unit length [8, 70, 71, 97, 110]. The total internal energy is the sum of the internal energy in each crease line, so:

$$E = \frac{1}{2}\sum_i l_{F,i}\, k_{t,i} (\psi_i - \psi_i^0)^2 \tag{1.1}$$

where $l_{F,i}$ is the length of the crease line, ψ_i is the angle between the facets and ψ_i^0 is the rest angle of the crease.

Origami sheets could by fabricated using a mold with the same pattern [44], or by plastic deformation of a flat sheet into the desired pattern. In the latter case, the sheet will undergo large deformations and there will be plastic deformations at the crease. Residual stresses are introduced, which may result in non-linear crease bending behavior, however, Lechenault et al. [42] shows that also in these cases, the crease behaves as a linear spring for a large range of angles.

1.2. Metamaterials

Metamaterials are materials with physical properties that are not found in nature and are typically made from small individual elements that are arranged in periodic spatial patterns [108]. These materials could have unusual optical [92], acoustic [47], thermal [7] or mechanical [80] behaviors.

The typical example of an optical metamaterial is a material with negative refractive index, which was introduced by Veselago in 1968 [92, 101, 108]. When light enters a slower medium with this property, it will refract in an unusual way, which could for example be used for superlenses that can measure beyond the diffraction limit [60] or for cloaking devices [60, 101]. A special class of optical metamaterials are the photonic crystals or photonic bandgap materials, which block the propagation of a band of frequencies of light in the structure, resulting in a band gap [75].

Similar to optical metamaterials, there are also acoustic metamaterials. These are artificially created materials, which are designed to control the propagation of elastic or phonon waves. Research on these acoustic metamaterials was inspired by optical metamaterials and shows a lot of similarities.

Applications for acoustic metamaterials are similar to those of optical metamaterials, as acoustic metamaterials could for instance be used for superlenses [1] (for acoustic imaging) and acoustic cloaking [11]. In addition, metamaterials could be engineered with great energy absorption properties [52, 108] (for instance by adding small resonators) and they could also be used to block elastic waves from propagating trough the structure for certain ranges of frequencies and resulting in a band gap [9, 45, 69, 108]. Resonant modes leads to exceptional reduction in sound transmission [3] and as a result certain ranges of frequencies are not able to propagate in the system and a band gap is formed.

These band gaps are usually accomplished by designing an artificial material with periodic variation of scatters (inclusions) with different acoustic properties than the background matrix. These metamaterials with scatters are defined as phononic crystals and are a special class of acoustic metamaterials. According to Yi et al. [105], the band gaps are the most important characteristic of acoustic metamaterials, as this property is considered to be the most fundamental property of acoustic metamaterials. Once these band gaps are known, they could be used for practical uses, for instance in acoustic filters, soundshields, acoustic waveguides, and transducers [69].

The origami materials, especially the Miura-ori pattern, has been proposed several times as a promising metamaterial. According to Surjadi et al. [80], the folding of sheets may lead to desirable mechanical properties such as multistability, extra large deformations, programmable stiffness, static morphing and negative Poisson's ratio [71, 97]. The Miura-ori pattern has also been proposed for materials with tunable termal expansion [7].

1.2.1. Examples of phononic crystals

Phononic crystals can be one, two, or three dimensional and are typically made of two elastic materials. These two materials form a cell that is periodically repeated in the metamaterial. The property of periodicity leads to constructive or destructive interference and are strongly related to the geometry of the structure and the frequency of the waves. Besides, the choice of the two materials also has an effect on the propagation of the wave through the structures. A high contrast between densities, elastic modulus and wave speeds in the two materials generally leads to a band gap [105].

An example of a classical phononic crystal in two-dimensions are solid cylinders in a solid background material. This type of crystal is for instance studied by Signalas and Economou [19, 76], and Kushwaha et al. [36, 37].

Over the years, some variations on these solid-solid cylinder type phononic crystals have been investigated. For instance, by using another state of matter for either the inclusion, background material, or both. Pennec et al. [61] studied some solid-solid, fluid-fluid, and solid-fluid phononic crystals. For instance: cylinder in air, water (resp. mercury) cylinders in mercury (resp. water) background, and steel cylinders in a epoxy resin matrix. In all these cases, a high contrast between the physical properties seem to be a general rule for the existence of a complete band gap [61].

Alternatively, a band gap is in some cases also found by changing the alignment or size of the cylinders, or by introducing vacancies in the cylinder array [61]. By using topology optimization, some more complex designs could be made, both regarding the unit-cell and the arrangement of multiple unit cells in the background material [105].

Most of these phononic crystals consider latitudinal and transverse waves only, however phononic band gaps also occur for flexural vibrations. For example: a study by Wen et al. [98] shows that a beam with alternating cross section and material, will also have a band gap in the dispersion relation, which could for

instance be used for vibration isolation.

1.2.2. Origami inspired acoustic metamaterials

Origami inspired structures seem to be a good candidate for acoustic metamaterials. Studies by Thota et al. [84–87] show that by attaching cylindrical inclusions on top of origami sheet acoustic waves could be guided or blocked. The origami sheet is used to tune the distance between the cylinders and the lattice topology, such that the band structure or wave propagation changes. These phononic structures resembles the classical cylinder in (solid) background material, but have the advantage that the wave propagation behavior could be tuned.

Tubes made from folded sheets could also be used to block a range of frequencies from propagating. For instance using a tube with a derivative of the Yoshimura pattern; the Triangulated Cylindrical Origami (TCO) pattern [103, 104], and also for tubes composed of the Tachi-Miura Polyhedron [102]. As these tubes do not have scatters in their structure, they are technically not phononic crystals. Acoustic metamaterial is therefore a better term to describe these materials with a band gap.

Wave propagation through undulated and folded sheets are relatively less studied, but these could be used as acoustic metamaterials. An out of plane component leads to coupling of modes that are otherwise orthogonal to one another [12, 88]. This could lead to a "modal" bandgap, where specific families of modes are forbidden, for example for undulated plates [88]. It could also lead to complete bandgaps, in case of folded structures, specifically for zig-zag folded beams [54] and homogeneous Miura-Ori and Eggbox patterns [65].

The advantage of these folded structures is that the size of the band gap could be tuned by the simple act of folding and that they are made from one single material. The size could additionally also be changed by modifying material properties, for instance the crease stiffness [54]. Introducing dislocations [77], may also influence the size of the band gap.

1.3. Wave propagation analysis methods

There are several methods to numerically predict the band structure. According to Zhao et al. [108] and Yi et al. [105], plane-wave expansion (PWE) method [39, 96, 99], finite difference time domain (FDTD) method [66, 78], multiple scattering theory (MST) [5, 33, 45, 46] and finite element method (FEM) [2, 17] are commonly used. Studies by Nanda and Karami [54], Pratapa et al. [64, 65], and Yasuda et al. [102] all use a truss based analysis for the propagation of waves in folded structures. So to summarize, the following methods are used to predict band structures:

- **Plane-wave expansion (PWE) method**, is used for regular periodic systems, and uses Fourier expansion for describing the material constants. It is an highly efficient method for calculating the band structure in periodic materials, due to its simplicity and ease of implementation. However, as this method relies on Fourier series expansion, it has some convergence issues. Especially when dealing with a high contrast in elastic material properties, which is typically the case in phononic crystals. As a large number of plane waves are then required, this method is both expensive and time consuming. It also uses the assumption of an infinite periodic material and cannot be used for finite phononic crystals [105]. The PWE method cannot be used if the inclusion is a nonviscous fluid or vacuum which does not support the propagation of transverse waves [82]. This method is used in a study by Trainiti et al. [88] for undulated plates and beams.

- **Finite difference time domain (FDTD) method**, this method uses finite difference approximations for both the space and time domains [105]. The numerical scheme is very popular for many problems in electromagnetics, as it is especially effective for the simulation of large-scale finite complex systems [82]. However the method requires a sufficient time discretization and is therefore generally time consuming, but Cao et al. showed that the computational time could be largely reduced by starting from the appropriate initial conditions [10].

- **Multiple scattering theory (MST)**, similar to the FDTD method, the MST can also be used for problems with a high contrast in elastic properties [10]. The MST is based upon the Korringa-Kohn-Rostoker method [34, 35], which is a well known method for the calculation of electronic band structures. In the MST, appropriate boundary conditions are applied on the boundary between the embedded particles and the background material. The method has excellent convergence for spherical and cylindrical inclusions, however it can only be used for systems with spherical or cylindrical scatters [105], so not for origami inspired crystals.

- **Finite element method (FEM)**, the most widely used method for prediction of the band structure, due to its relatively high computational efficiency [108]. The method was initially proposed for finding solutions for structural mechanics problems, but can also be used for other initial and boundary value problems. The method uses the Floquet-Bloch theory [6, 22] to obtain a generalized eigenvalue problem of the form $A\mathbf{u} = \omega^2 B\mathbf{u}$, which is then solved by a eigenvalue solver. Most studies use a conforming mesh, but an extended formulation for the finite element method (XFEM) has also been proposed for the prediction of band gaps [108], such that there is no need for a conforming mesh. A study by Trainiti et al. [88] showed that the finite element method could be used for the wave propagation in undulated beams. They also argue that this method could be used for more complex deformation characteristics, such as shear deformation trough the thickness of the beam.

- **Truss-based analysis**, is specifically for folded structures. Studies by Nanda and Karami [54], Pratapa et al. [64, 65], and Yasuda et al. [102] all use a truss based analysis for the propagation of waves in folded structures. The geometry in these truss based analysis is represented as a combination of bars and hinges, an example for the Miura-ori sheet is shown in Fig. 1.2. Rotational springs are added on the fold lines and at the middle of the plate where the face is allowed to bend. Similar to the finite element method, the Floquet-Bloch wave framework is used to obtain a generalized eigenvalue problem, which is then solved.

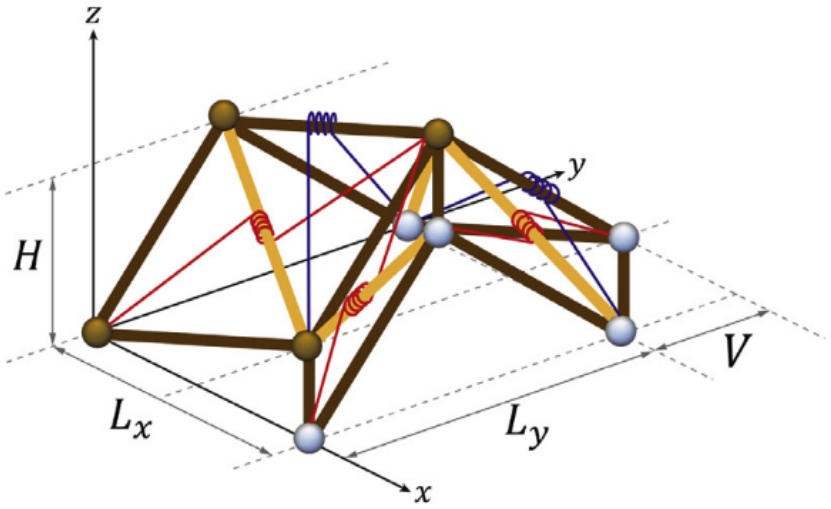

Figure 1.2: Bar and hinge representation of the Miura-ori unit cell. The bars along the fold lines are dark brown, the lighter bars are along the lines where the sheet is allowed to bend. Rotational springs are added at the bend lines (red) and at the fold lines (blue). [65]

To summarize, according to Zhao et al., the finite element method is the most widely used due to its relatively high computational efficiency [108]. However, it is still a computational expensive process to perform an optimization process to obtain a desired band structure, as this would require frequent re-meshing of the geometry in order to ensure a conforming mesh. The truss-based analysis has the advantage that they minimize the degrees of freedom, and are therefore less expensive.

However, the bar and hinge method also have some limitiations. The deformation modes are first of all predominantly axial [65], which in return has an effect on the band structure, especially for higher frequencies. Secondly, stiffness for shearing of the panels is overestimated in comparison to stretching and bending [21], and finally the bar and hinge models has a lower design flexibility, as they cannot be used independently from geometry. The bar and hinge models can currently only model quadrilateral and triangular panels [21]. To overcome these issues, we propose to use the Finite Element Method (FEM) with shell elements instead, as this will allow for a more accurate representation of the structures, without the aforementioned limitations. Besides, the Finite Element Method could in theory be used for any kind of panel or structure, including arbitrary polygonal panels and structures with dislocations.

1.4. Band gap

The propagation of waves in periodic structures was first studied by Floquet [22] and later generalized by Bloch [6] for three dimensions, and is now known as *Floquet-Bloch theory* or *Bloch theorem* [105]. According to this theorem, all fields in an infinite periodic solid can be expanded to infinite bases, for example for field $h(\mathbf{x}, t)$ [108]:

$$h(\boldsymbol{x}, t) = \sum_{\boldsymbol{k}} h_{\boldsymbol{k}}(\omega, \boldsymbol{k}) e^{i(\omega t - \boldsymbol{k}\cdot\boldsymbol{x})}, \tag{1.2}$$

where $\boldsymbol{k}$ is the Floquet-Bloch wave vector and $\omega = \omega(\boldsymbol{k})$ the frequency of the wave vector. For the displacement field, this relation becomes:

$$\boldsymbol{u}(\boldsymbol{x}, t) = \bar{\boldsymbol{u}}_{\boldsymbol{k}}(\omega, \boldsymbol{k}) e^{i(\omega t - \boldsymbol{k}\cdot\boldsymbol{x})} \tag{1.3}$$

where $\bar{\boldsymbol{u}}$ is the periodic magnitude of the displacement field for a given wave vector $\boldsymbol{k}$ and frequency ω. The periodic magnitude is defined for the unit cell of the structure.

A solid body with a periodic structure can be characterized by the translation of a unit cell with a translation or periodicity vector $\mathbf{T} = n_i \mathbf{a}_i$, where $\mathbf{a}_1, \mathbf{a}_2, \mathbf{a}_3 \in \mathbb{R}^3$ are the lattice vectors of the structure and n_1, n_2, n_3 are arbitrary integers. In some cases a finite periodic solid is considered [65], in these cases the possible values for n_i will be a finite set of integers.

Substitution of $\boldsymbol{x} = \boldsymbol{x} + \mathbf{T}$ into Eq. (2.9), will give an expression for the displacement field of the translated unit cell, see Eq. (2.10). Substitution of Eq. (2.9), will yield a simpler expression.

$$\boldsymbol{u}(\boldsymbol{x} + \mathbf{T}, t) = \bar{\boldsymbol{u}}_{\boldsymbol{k}}(\omega, \boldsymbol{k}) e^{i(\omega t - \boldsymbol{k}\cdot(\boldsymbol{x}+\mathbf{T}))} = \boldsymbol{u}(\boldsymbol{x}, t) e^{-i\boldsymbol{k}\cdot\mathbf{T}} \tag{1.4}$$

The displacement field for the translated cell can thus be deducted using the displacement field of the original cell. It is therefore sufficient to only consider the displacement field of a single cell, which leads to large savings for wave propagation analysis in periodic structures.

We can then define a reciprocal lattice, which is a lattice in Fourier space that is associated with the unit cell [32]. The primitive vectors of the reciprocal lattice are constructed using the lattice vectors $\mathbf{a}_1, \mathbf{a}_2, \mathbf{a}_3$, by satisfying the condition $\mathbf{b}_i \cdot \mathbf{a}_i = 2\pi\delta_{ij}$, which will result in the following reciprocal lattice vectors [32]:

$$\mathbf{b}_1 = 2\pi \frac{\mathbf{a}_2 \times \mathbf{a}_3}{\mathbf{a}_1 \cdot \mathbf{a}_2 \times \mathbf{a}_3}, \qquad \mathbf{b}_2 = 2\pi \frac{\mathbf{a}_3 \times \mathbf{a}_1}{\mathbf{a}_1 \cdot \mathbf{a}_2 \times \mathbf{a}_3}, \qquad \mathbf{b}_3 = 2\pi \frac{\mathbf{a}_1 \times \mathbf{a}_2}{\mathbf{a}_1 \cdot \mathbf{a}_2 \times \mathbf{a}_3}, \tag{1.5}$$

Origami plates have periodicity in only two dimensions, so for these cases, the reciprocal lattice vectors reduces to:

$$\mathbf{b}_1 = 2\pi \frac{\mathbf{R}\mathbf{a}_2}{\mathbf{a}_1 \cdot \mathbf{R}\mathbf{a}_2}, \qquad \mathbf{b}_2 = 2\pi \frac{\mathbf{R}\mathbf{a}_1}{\mathbf{a}_2 \cdot \mathbf{R}\mathbf{a}_1} \tag{1.6}$$

where $\mathbf{R}$ is the 90 degree rotation matrix.

The wave vector $\boldsymbol{k}$ in the reciprocal lattice can be expressed as:

$$\boldsymbol{k} = k_1 \mathbf{b}_1 + k_2 \mathbf{b}_2 + k_3 \mathbf{b}_3 \tag{1.7}$$

For the wave vector we generally choose a vector that lies in the first Brillouin zone, as it can be shown that this is sufficient for describing all elastic waves. For any wave vector outside the first Brilouin zone, one would simply subtract an appropriate reciprocal lattice vector $\mathbf{G} = \nu_i \mathbf{b}_i$, where the Einstein notation is used and ν_i are arbitrary integers. By taking all the symmetries of the lattice into account, it is possible to use an even smaller zone: the irreducible Brillouin zone. This zone is for example used in the dispersion relation, where the wavevector makes a loop over the boundary of the irreducible Brillouin zone. The wavevector would for example take the path $\Gamma - X - M - \Gamma$ in Fig. 1.3b.

The first Brillouin zone is a special type of unit cell in reciprocal space, see Fig. 1.3a for instructions on how to draw this zone. According to Kittel [32], the first Brillouin zone is defined as the smallest volume that is enclosed by planes that are perpendicular bisectors of the reciprocal lattice vectors. The first Brillouin zone is a Wigner-Seitz cell in reciprocal space.

Figure 1.4a shows the direct lattice of the Miura-Ori pattern, which is spanned by the lattice vectors $\mathbf{a}_i$. The corresponding reciprocal lattice is shown in Fig. 1.4b, in which the first Brillouin zone is the area enclosed by {Q",Q',Q,R'}. The irreducible Brillouin zone is the zone enclosed by {O, P, Q, R}. The irreducible Brillouin

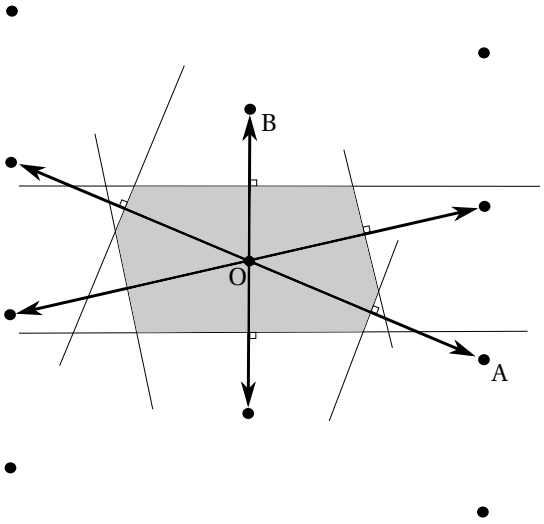

(a) An example of the creation of the first Brillouin zone in two dimensions. First draw vectors from O to nearby points (e.g. A and B), then intersect in the middle and construct lines perpendicular to the drawn vectors. The smallest enclosed area is the first BrillouinZone. [32]

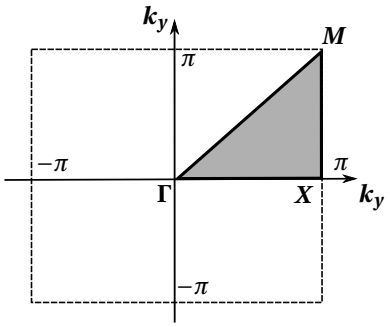

(b) The irreducible Brillouin zone for a unit cell with square geometry. $\boldsymbol{\Gamma}$, $\boldsymbol{X}$ and $\boldsymbol{M}$ are the critical points.

Figure 1.3: The first Brillouin zone and irreducible Brillouin zone

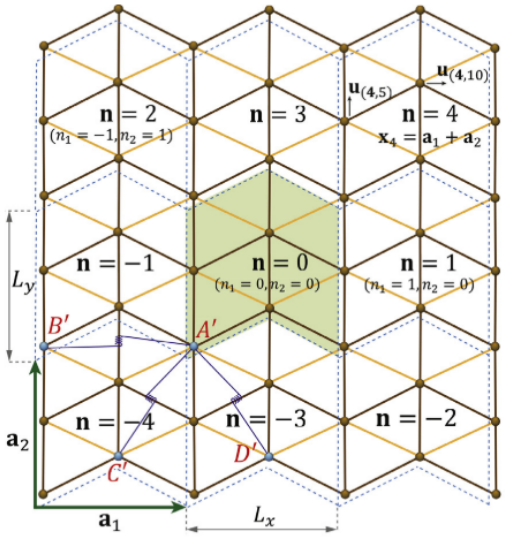

(a) The direct lattice for a Miura-ori sheet. The dashed lines represents the boundary of the individual cells. [65]

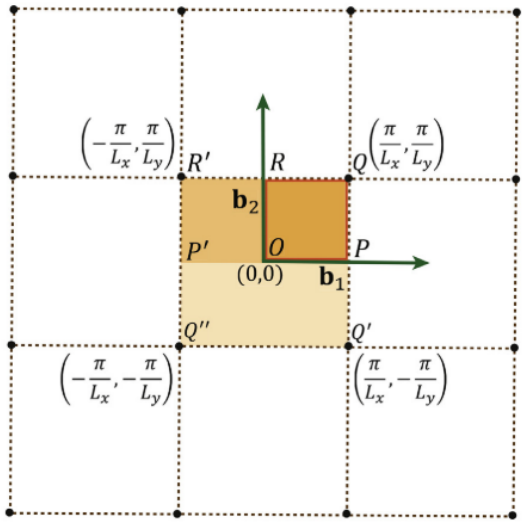

(b) The corresponding reciprocal lattice for the Miura-Ori pattern. The zone enclosed by {Q",Q',Q,R'} is the first Brillouin zone, the zone enclosed by {O, P, Q, R} is the irreducible Brillouin zone. [65]

Figure 1.4: The direct and reciprocal lattice of the Miura-Ori pattern.

zone was found by applying time-reversal and spatial symmetry, the details of the reduction can be found in Pratapa et al. [65].

The balance of momentum in absence of external forces and damping is:

$$\mathbf{M}\ddot{\mathbf{U}} + \mathbf{K_t}\mathbf{U} = 0 \tag{1.8}$$

where $\mathbf{K_t}$ is the tangential stiffness matrix, $\mathbf{M}$ is the mass matrix and $\mathbf{U}$ the vector with nodal displacements. Using Eq. (2.9), Eq. (1.8) can be rewritten as:

$$\left(\mathbf{K_t} - \omega^2\mathbf{M}\right)\mathbf{U} = 0 \tag{1.9}$$

this is an eigenvalue problem and solving it will give the modal frequencies $\omega_i (i = 1,2,3,\ldots,n_m)$ for corresponding wave vector $\mathbf{k}$. Plotting the wave vector in the Irreducible Brillouin Zone (IBZ) versus the (normalized) modal frequencies, will give an dispersion diagram as show in Fig. 1.5, as was done by Pratapa et al. [65]. The band gap, in which waves cannot propagate through the structure is shown in gray for the Miura-Ori pattern. Similar results were also found for the Eggbox pattern.

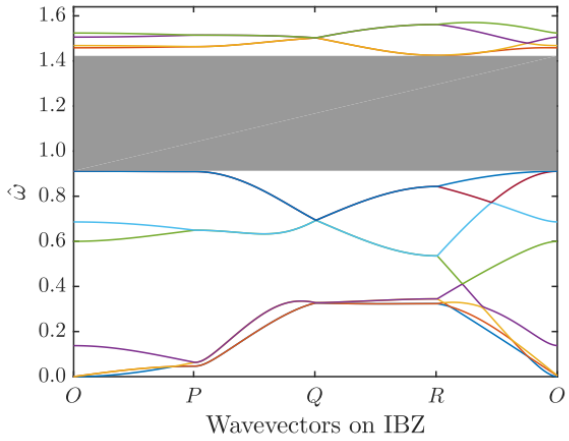

Figure 1.5: Band structure diagram for a Miura-Ori sheet, with $\alpha = 59.53°$, $b = 4.96$, and $\theta = 57.93°$ (see Fig. 2.1b for the geometric parameters) [65]. The wave vector in the Irreducible Brillouin Zone (IBZ) is plotted against the normalized frequency. The band gap is indicated in gray.

1.5. Research goal

We have seen that origami sheets can have a band gap in the band structure diagram, for example for the Miura-Ori pattern and the Eggbox pattern, and that these can for example be tuned by varying the angle of the fold or altering the stiffness of the creases.

However, for obtaining these band structure diagrams, the origami sheets were represented using a bar and hinge model. It is known that these limit the possible deformation modes to be predominantly axial, higher frequencies in the band structure diagram therefore cannot be represented accurately. Besides, stiffness for shearing of the panels is overestimated in comparison to stretching and bending. The last disadvantage of these bar and hinge models is that these cannot be represented independent from geometry and can thus far only be used for origami sheets with quadrilateral and triangular panels.

To overcome these issues, we propose to use the Finite Element Model (FEM) with shell elements instead, as this will allow for a more accurate representation of the structures, without the aforementioned limitations. Besides, the Finite Element Method could in theory be used for any kind of panel or structure, including arbitrary polygonal panels and structures with dislocations.

The finite element method, would therefore allow one to design new origami patterns with desired wave propagation characteristics, which may have some relevant new applications in the field of vibrations and acoustics. Getting more insight in the geometrical and material parameters that define the vibration isolation characteristics would therefore be an essential first step in the exploration of new origami acoustic metamaterials.

A logical first step is to start with the well known Miura-ori pattern, for which a band gap has already been found with a bar and hinge model, and check whether the same band is also found when using the finite element model. On this pattern one could then study the effects of changing the geometrical and material properties. For instance tuning the crease stiffness, which has so far only been done for a 1D strip, and not yet for 2D origami patterns.

This leads us to the following research question:

> What causes a band gap to form in origami sheets and how can these be used for tunable vibration isolation?

This question is answered by answering the following sub questions:

1. What is the effect of the crease stiffness on the band gap of the Miura-Ori pattern?
2. How does the geometry of the Miura-Ori pattern influence the size of the band gap?
3. What is the effect of folding on the size on the vibration isolation characteristics?

1.6. Outline

In this section, a brief outline of the thesis is presented. The main results and answers the above mentioned research questions can be found in the form of a paper in Chapter 2. In Chapter 3, some recommendations were listed that were detected during the project. It also lists some recommendations for future work. The main content is ended in Chapter 4, with a personal reflection on the whole project. At the end of the report there are some appendices, with content that did not fit in the general chapters.

2

Paper

Unintended vibrations are present in almost all mechanical systems and can have disruptive or destructive effects. They may for instance prevent obtaining accurate measurements, may lead to a breakdown of a structure, or have any other undesired effect. Therefore, approaches to get rid of these unwanted vibrations are desired.

There are various approaches to filter unintended vibrations, for instance by choosing proper materials which dampen the vibrations, through active noise canceling or by using destructive interference, in this paper we will focus on the latter one.

A class of materials that utilizes destructive interference through Bragg scattering are the Phononic Crystals (PnCs). They are typically made from unit cells with two elastic materials that are periodically repeated in the metamaterial, for example, solid cylinders in a solid background material [12, 17, 19, 36, 37, 76, 82]. Variations on these PnCs could be made by using other states of matter [10, 61], introducing vacancies [61], or by using other alignments [61]. The phononic crystals are not limited to 2D or 3D solids, also beams [98, 100, 106, 107] and (folded) plates [23, 64, 76] were proposed. High contrast between the two elastic materials generally lead to a bandgap in the band structure (or dispersion relation) [105], in which waves with a certain range of frequencies are not able to propagate through the material. Because of these bandgaps, PnCs have many applications, for instance in acoustic filters, soundshields, acoustic waveguides, transducers, but also in vibration isolation [69].

Phononic Crystals are all structures where the material properties are modulated on a scale comparable to the wavelength of the acoustic waves. Acoustic metamaterials (AMs) are similar to PnCs but are distinguished by their sub-wavelength periodicity [47]. Individual resonance from single unit cells and its interaction with Bragg resonance may lead to interesting wave phenomena. An accepted definition of AMs does not yet exist, some researchers include PnCs in AMs, others do not [47].

Most of the work on PnCs and AMs is for passive control of wave propagation [30, 95]. It may, however, be practical to seek a PnC or AM where the propagation can be actively controlled or tuned, as this would open up more applications. This could, for instance, be done using piezoelectricity [30], magnetism [30], temperature [30], or finite elastic deformation [26, 30], however, in this study we use folded structures (origami) for the active control of wave propagation, which has the advantage that the act of folding is relatively simple compared to other means of active noise canceling.

Origami—the Japanese art of folding paper in decorative shapes and figures—originated from the Japanese words for fold (oru) and paper (kami) [41], and has gained attention in recent years from scientists and engineers who try to use the folding of plates for technological applications. Literature studies [43, 89] list several of these applications, which include for example packaging, deployable (space) structures, biomedical devices, robotics, and architectural structures.

The most well-known and most studied origami pattern is the Miura-Ori pattern, named after K. Miura. The pattern was invented for the easy deployment of solar panel arrays in space [53] and later studied for its remarkable material properties. The pattern is flat foldable and has a negative Poisson's ratio for in-plane deformations [71]. The negative Poisson's ratio property is not found naturally in nature, which makes the Miura-Ori a metamaterial.

Previous studies have already used the propagation of waves. By attaching cylinders to Miura-Ori sheets [84–87], where the origami is used to tune the distance between cylinders and thus the lattice topology. Al-

ternatively, one could use origami tubes, for either vibration absorption (tubes composed of the Triangulated Cylindrical Origami (TCO) pattern [103, 104] or the Tachi-Miura Polyhedron [102]) or for sound absorption [31].

Wave propagation through undulated and folded sheets are less studied, but these could be used as acoustic metamaterials. An out-of-plane component leads to coupling of modes that are otherwise orthogonal to each other [12, 88]. This could lead to a *modal* bandgap, where specific families of modes are forbidden, for example for undulated plates [88]. It could also lead to complete bandgaps, in the case of folded structures, specifically for zig-zag folded beams [54] and homogeneous Miura-Ori and Eggbox patterns [65]. In these structures, the size of the bandgap could be tuned simply by folding the material. Additionally, the size could also be changed by modifying material properties, for instance, the crease stiffness [54]. Introducing dislocations [77] may also influence the size of the bandgap. An added benefit is that these structures are made from one single material, which may be practical when manufacturing.

For the band structure of the Miura-ori and Eggbox patterns, a bar and hinge method was used [65]. However, these models have some limitations. First of all, the deformation modes are predominantly axial [65], which in return affects the band structure, especially for higher frequencies. Secondly, stiffness for shearing of the panels is overestimated in comparison to stretching and bending [21]. And finally, the bar and hinge models can currently only model quadrilateral and triangular panels [21]. To overcome these issues, we propose using the Finite Element Method (FEM) with shell elements instead, as this will allow for a more accurate representation of the structures without the aforementioned limitations. Furthermore, the Finite Element Method could in theory be used for any kind of panel or structure, including arbitrary polygonal panels and structures with dislocations.

The paper is organized as follows. First, the unit cell geometries of the two structures, a zig-zag folded strip and Miura-Ori pattern, are introduced. Secondly, we describe the various methods that were used to analyze these structures. We then use these methods and propose a theory why bandgaps may form in zig-zag structures and then apply this for the Miura-Ori sheets. Next, we discuss the various band structure characteristics of two found (local) optima of the Miura-Ori sheet. And finally, we end the study with some concluding remarks.

2.1. Configurations and geometry

The two structures that are used in this paper can be rigid folded along pre-specified crease lines, where the bending stiffness may be lower than in the surrounding material. For paper, this is trivially achieved with the folding of the paper itself. For other materials (like metals), one may artificially weaken the structure by, for instance, removing material from the fold locations.

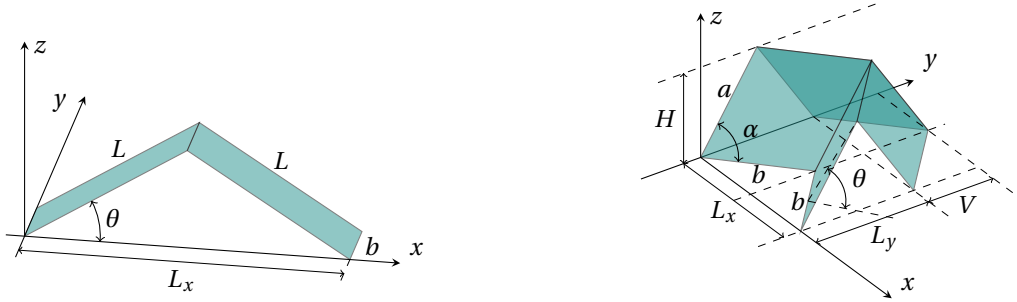

(a) Unit cell of a zig-zag folded strip.

(b) Unit cell of the Miura-ori sheet.

Figure 2.1: Geometry of a unit cell of the zig-zag folded strip (a) and the Miura-ori sheet (b), in terms of edge lengths L, a and b, fold angle $\theta \in [0, \pi/2]$ and parallellogram or panel angle $\alpha \in [0, \pi/2]$. Outer dimensions H, L_x, L_y and V are shown, if applicable.

A unit cell of the zig-zag folded strip is shown in Fig. 2.1a. This unit cell is periodically repeated only in the x direction. The unit cell consists of two beams with length L, which are on either side connected via torsional springs with stiffness per unit length k_t. These springs represent the folds of the strip. The zig-zag folded strip has width b, thickness t, and a fold angle $\theta \in [0, \pi/2]$.

We make the zig-zag folded strip dimensionless by normalizing the dimensions with the length in the x-direction L_x in the flat configuration ($\theta = 0$). The fold stiffness k_t can be made dimensionless, using fold length b and the flexural rigidity $D = Et^3/(12(1-\nu^2))$. The band frequencies ω are presented in a non-dimensional form by normalizing with the speed of the longitudinal waves $c_L = \sqrt{\frac{E}{\rho(1-\nu^2)}}$ [88] and the length

in the x-direction for the flat configuration ($L_x = 2L$):

This results in the following dimensionless parameters:

$$\zeta = \frac{b}{2L}, \qquad \gamma = \frac{t}{2L}, \qquad \eta = \frac{k_t b}{D}, \qquad \Omega = \frac{\omega 2L}{c_L}. \tag{2.1}$$

The geometry of the unit cell of a Miura-Ori sheet is shown in Fig. 2.1b. The unit cell consists of four identical panels, which are defined by edge lengths a and b and panel angle α. The unit cell is folded from a flat configuration with a fold angle $\theta \in (0, \pi/2]$. The sheet has thickness t and at the edges between the panels, there are additional rotational springs with stiffness k_t per unit length, which represent a fold or crease. A Miura-Ori sheet is created by repeating the unit cell in both x and y directions. The outer dimensions of the unit cell are given by [65, 71]

$$H = a \sin\theta \sin\alpha, \tag{2.2}$$

$$L_x = 2b \frac{\cos\theta \tan\alpha}{\sqrt{1 + \cos^2\theta \tan^2\alpha}}, \tag{2.3}$$

$$L_y = 2a\sqrt{1 - \sin^2\theta \sin^2\alpha}, \tag{2.4}$$

and

$$V = b \frac{1}{\sqrt{1 + \cos^2\theta \tan^2\alpha}}. \tag{2.5}$$

The cell is made dimensionless by normalizing both the edge length b and the sheet thickness t with the edge length a. The stiffness of the crease is normalized with the flexural rigidity D and edge length a, and the band frequencies ω are presented in a non-dimensional form by normalizing with the speed of the longitudinal waves c_L and the edge length a.

$$\zeta = \frac{b}{a}, \qquad \gamma = \frac{t}{a}, \qquad \eta = \frac{k_t a}{D}, \qquad \Omega = \frac{\omega a}{c_L}. \tag{2.6}$$

2.2. Floquet-Bloch theorem

In this work, we analyze infinite periodic elastic structures, using the finite element method, where periodic boundary conditions are applied using the Floquet-Bloch theorem or simply Bloch theorem [105].

The infinite periodic structure can be characterized by the translation of a periodic unit cell (PUC) with a translation or periodicity vector $\mathbf{T} = n_i \mathbf{a}_i$ (using Einstein notation), where $\mathbf{a}_1, \mathbf{a}_2, \mathbf{a}_3 \in \mathbb{R}^3$ are the lattice vectors of the structure and n_1, n_2, n_3 are arbitrary integers. We can then define a reciprocal lattice, which is a lattice in Fourier space that is associated with the unit cell [32]. The primitive vectors of the reciprocal lattice are constructed using the lattice vectors $\mathbf{a}_1, \mathbf{a}_2, \mathbf{a}_3$, by satisfying the condition $\mathbf{b}_i \cdot \mathbf{a}_i = 2\pi\delta_{ij}$, which will result in the following reciprocal lattice vectors [32]:

$$\mathbf{b}_1 = 2\pi \frac{\mathbf{a}_2 \times \mathbf{a}_3}{\mathbf{a}_1 \cdot \mathbf{a}_2 \times \mathbf{a}_3}, \qquad \mathbf{b}_2 = 2\pi \frac{\mathbf{a}_3 \times \mathbf{a}_1}{\mathbf{a}_1 \cdot \mathbf{a}_2 \times \mathbf{a}_3}, \qquad \mathbf{b}_3 = 2\pi \frac{\mathbf{a}_1 \times \mathbf{a}_2}{\mathbf{a}_1 \cdot \mathbf{a}_2 \times \mathbf{a}_3}, \tag{2.7}$$

For two dimensions, this reduces to:

$$\mathbf{b}_1 = 2\pi \frac{\mathbf{R}\mathbf{a}_2}{\mathbf{a}_1 \cdot \mathbf{R}\mathbf{a}_2}, \qquad \mathbf{b}_2 = 2\pi \frac{\mathbf{R}\mathbf{a}_1}{\mathbf{a}_2 \cdot \mathbf{R}\mathbf{a}_1} \tag{2.8}$$

where $\mathbf{R}$ is the 90 degree rotation matrix.

The wave vector $\boldsymbol{k}$ is a linear combination of the primitive vectors of the reciprocal lattice, so $\boldsymbol{k} = k_i \mathbf{b}_i$. We generally choose a vector that lies in the first Brillouin zone, as it can be shown that this is sufficient for describing all elastic waves [63]. For any wave vector outside the first Brillouin zone, one would simply subtract an appropriate reciprocal lattice vector $\mathbf{G} = v_i \mathbf{b}_i$, where Einstein notation is used and v_i are arbitrary integers. By taking all the symmetries of the lattice into account, it is possible to use an even smaller zone: the irreducible Brillouin zone. This zone is for example used in the band structure, where the wave vector makes a loop over the boundary of the irreducible Brillouin zone.

The two-dimensional origami lattice is generally either rectangular or square and of primitive type. Special attention is required when the lattice is square because origami patterns generally do not have inversion symmetry and thus additional paths may be required. Using the conventions from [28, 74], the recommended path along the IBZ is $\Gamma - X - S - Y - \Gamma$.

According to the Bloch theorem, all fields in an infinitely periodical solid can be expanded to infinite bases, for example the displacement $\boldsymbol{u}(\boldsymbol{x}, t)$ [108]:

$$\boldsymbol{u}(\boldsymbol{x}, t) = \boldsymbol{U}(\boldsymbol{x}) e^{i(\omega t - \boldsymbol{k}\cdot\boldsymbol{x})}, \tag{2.9}$$

where $\boldsymbol{U}(\boldsymbol{x})$ is the periodic magnitude of the displacement field for a given Floquet-Bloch wave vector $\boldsymbol{k}$ and frequency $\omega = \omega(\boldsymbol{k})$. The periodic magnitude is defined for the unit cell of the structure and has the same periodicity as the medium.

Substitution of $\boldsymbol{x} = \boldsymbol{x} + \mathbf{T}$ into Eq. (2.9), will give an expression for the displacement field of the translated periodic unit cell:

$$\boldsymbol{u}(\boldsymbol{x} + \mathbf{T}, t) = \boldsymbol{U}(\boldsymbol{x}) e^{i(\omega t - \boldsymbol{k}\cdot(\boldsymbol{x}+\mathbf{T}))} = \boldsymbol{u}(\boldsymbol{x}, t) e^{-i\boldsymbol{k}\cdot\mathbf{T}}, \tag{2.10}$$

The displacement field for the translated cell can thus be deducted using the displacement field of the original cell. It is therefore sufficient to only consider the displacement field of a single cell, which leads to large savings for wave propagation analysis in infinite periodic structures. Given this property and using a Galerkin method, we can discretize the unit cell and obtain the equations of motion as:

$$\boldsymbol{M}\ddot{\boldsymbol{U}} + \boldsymbol{K}(\boldsymbol{k})\boldsymbol{U} = \mathbf{0}, \tag{2.11}$$

where $\boldsymbol{K}$ is the stiffness matrix, $\boldsymbol{M}$ is the mass matrix, and $\boldsymbol{U}$ is the nodal displacement vector. Using a dimensionless time $\tau = \omega t$ and assuming solutions of the form $\boldsymbol{U} = \frac{A}{2}\boldsymbol{\phi}_j e^{i\tau}$, yields a generalized eigenvalue problem $(\boldsymbol{K}(\boldsymbol{k}) - \omega^2\boldsymbol{M})\boldsymbol{\phi}_j = \mathbf{0}$ which can be solved for eigenvalues ω_j^2 and eigenvectors $\boldsymbol{\phi}_j$. Solving this generalized eigenvalue problem for all wavevectors $\boldsymbol{k}$ on the irreducible Brillouin zone, yields a band structure diagram for a linear structure.

2.3. Complex band

The previously described method for obtaining the band structure can be considered to be the $\omega(\boldsymbol{k})$ approach and results in a band structure that is real-valued, *i.e.*, provides only the set of purely propagative waves that are supported by the media [58]. However, periodic media can support evanescent modes as well, which are never predicted by the classical $\omega(\boldsymbol{k})$ methods. Evanescent modes are particular solutions of the wave equation that decay or increase exponentially with distance and are characterized by the fact that the wave vector $\boldsymbol{k}(\omega)$ is complex-valued for a certain frequency ω. Bandgaps should then be defined as the ranges of frequencies where only evanescent modes can be excited [67, 68].

The imaginary part of the first harmonic has been linked to the decay of the amplitude of the propagating waves through the periodic structure [4, 67, 68]. Obtaining this imaginary part would thus give better insight into the filtering properties of the periodic structure.

To obtain complex solutions, one must use the $\boldsymbol{k}(\omega)$ approach [4, 18, 40, 48, 67, 68, 83, 90, 91, 109], were the unknown (complex) wave vectors $\boldsymbol{k}$ are solved for a fixed frequency ω and direction of incidence $\hat{\boldsymbol{k}}_n$.

The $\boldsymbol{k}(\omega)$ method generally requires the elimination of the inner degrees of freedom in the structure, which is a major disadvantage of the method as the required dynamic condensation is typically computationally demanding

The method for obtaining complex band structures was described by Veres *et al.* [91]. They divided the two dimensional finite element space into nine sets of nodes $\boldsymbol{v}_i$. These are the nodes on the four boundaries, the four corner nodes and the internal nodes. They then applied a dynamic condensation to get rid of internal DOFs, giving a reduced dynamic stiffness matrix [91].

The discretized equations of motion can be written as:

$$\left(\boldsymbol{K} - \omega^2\boldsymbol{M}\right) = \boldsymbol{D}\boldsymbol{v} = \begin{bmatrix} \boldsymbol{d}_{11} & \dots & \boldsymbol{d}_{19} \\ \vdots & \ddots & \vdots \\ \boldsymbol{d}_{19}^T & \dots & \boldsymbol{d}_{99} \end{bmatrix} \tag{2.12}$$

Applying dynamic condensation to get rid of the internal degrees of freedom $\boldsymbol{v}_4$:

$$\boldsymbol{D}_{red} = \boldsymbol{T}_1^T \boldsymbol{D} \boldsymbol{T}_1 - \boldsymbol{T}_1^T \boldsymbol{D} \boldsymbol{T}_2 \left(\boldsymbol{T}_2^T \boldsymbol{D} \boldsymbol{T}_2 \right)^{-1} \boldsymbol{T}_2^T \boldsymbol{D} \boldsymbol{T}_1 \tag{2.13}$$

where T_1 and T_2 are the transformation matrices, which are used to eliminate the inner degrees of freedom $\boldsymbol{v}_i = \boldsymbol{v}_4$ [91].

$$\boldsymbol{T}_1 = \begin{bmatrix} \boldsymbol{I}_{n_1} & \boldsymbol{0}_{n_1,n_2} \\ \boldsymbol{0}_{n_i,n_1} & \boldsymbol{0}_{n_i,n_2} \\ \boldsymbol{0}_{n_2,n_1} & \boldsymbol{I}_{n_2} \end{bmatrix} \tag{2.14}$$

and

$$\boldsymbol{T}_2 = \begin{bmatrix} \boldsymbol{0}_{n_1,n_i} \\ \boldsymbol{I}_{n_i} \\ \boldsymbol{0}_{n_2,n_i} \end{bmatrix} \tag{2.15}$$

where $\boldsymbol{I}$ and $\boldsymbol{0}$ are the identity matrix and the zero matrix. The subscripts n_1, n_i and n_2 indicate respectively the number of master, inner and slave DOFs. The dynamic reduction is expensive, alternatively one could use a modal reduction step, as proposed by Palermo et al. [58].

The transfer matrix approach is then used to apply the Bloch-Floquet periodic boundary conditions. We define the propagation constants $\lambda_x = e^{ik_x h_x}$ and $\lambda_y = e^{ik_y h_y}$, where k_x and k_y are the components of the two dimensional wave vector $\boldsymbol{k} = [k_x, k_y]^T$. We then assume that the wave vector is of the form $\mathbf{k} = \mathbf{k}_0 + \alpha \hat{\mathbf{k}}_n$ where $\hat{\mathbf{k}}_n$ is a unit vector, so $\hat{\mathbf{k}}_n \cdot \hat{\mathbf{k}}_n = 1$. Substitution gives:

$$\lambda_x = e^{ik_x h_x} = e^{ik_{0,x} h_x} e^{i\alpha \hat{k}_{n,x}} \tag{2.16}$$

$$\lambda_y = e^{ik_y h_y} = e^{ik_{0,y} h_y} e^{i\alpha \hat{k}_{n,y}} \tag{2.17}$$

The transfer matrices are defined as:

$$\boldsymbol{\Lambda}_R = \begin{bmatrix} \boldsymbol{I}_{m_1} & \boldsymbol{0} & \boldsymbol{0} \\ \boldsymbol{0} & \boldsymbol{I}_{m_2} & \boldsymbol{0} \\ \boldsymbol{0} & \boldsymbol{0} & \boldsymbol{I}_{m_3} \\ \lambda_y \boldsymbol{I}_{m_1} & \boldsymbol{0} & \boldsymbol{0} \\ \boldsymbol{0} & \lambda_x \boldsymbol{I}_{m_2} & \boldsymbol{0} \\ \boldsymbol{0} & \boldsymbol{0} & \lambda_x \boldsymbol{I}_{m_3} \\ \boldsymbol{0} & \boldsymbol{0} & \lambda_y \boldsymbol{I}_{m_3} \\ \boldsymbol{0} & \boldsymbol{0} & \lambda_x \lambda_y \boldsymbol{I}_{m_3} \end{bmatrix} \tag{2.18}$$

$$\boldsymbol{\Lambda}_L = \begin{bmatrix} \boldsymbol{I}_{m_1} & \boldsymbol{0} & \boldsymbol{0} \\ \boldsymbol{0} & \boldsymbol{I}_{m_2} & \boldsymbol{0} \\ \boldsymbol{0} & \boldsymbol{0} & \boldsymbol{I}_{m_3} \\ \lambda_y^{-1} \boldsymbol{I}_{m_1} & \boldsymbol{0} & \boldsymbol{0} \\ \boldsymbol{0} & \lambda_x^{-1} \boldsymbol{I}_{m_2} & \boldsymbol{0} \\ \boldsymbol{0} & \boldsymbol{0} & \lambda_x^{-1} \boldsymbol{I}_{m_3} \\ \boldsymbol{0} & \boldsymbol{0} & \lambda_y^{-1} \boldsymbol{I}_{m_3} \\ \boldsymbol{0} & \boldsymbol{0} & \lambda_x^{-1} \lambda_y^{-1} \boldsymbol{I}_{m_3} \end{bmatrix} \tag{2.19}$$

where m_1, m_2 and m_3 are the number of DOFs in respectively $\boldsymbol{v}_1, \boldsymbol{v}_2$ and $\boldsymbol{v}_3$. The reduced equations of motion are then written as:

$$(\boldsymbol{\Lambda}_L^T \boldsymbol{D}_{red} \boldsymbol{\Lambda}_R) \tilde{\boldsymbol{v}} = \tilde{\boldsymbol{D}} \tilde{\boldsymbol{v}} = \boldsymbol{0} \tag{2.20}$$

where $\tilde{\boldsymbol{v}} = [\boldsymbol{v}_1, \boldsymbol{v}_2, \boldsymbol{v}_3]^T$ is the reduced degree of freedom vector. Performing the multiplication between the matrices in Eq. (2.20), pre-multiplying by $\lambda_x \lambda_y$ and sorting by λ_x and λ_y, we can write the reduced equations of motion as:

$$\tilde{\mathbf{D}}\mathbf{v} = \left(\lambda_x^2 \lambda_y^2 \mathbf{K}_1 + \lambda_x^2 \lambda_y \mathbf{K}_2 + \lambda_x \lambda_y^2 \mathbf{K}_3 + \lambda_x^2 \mathbf{K}_4 + \lambda_x \lambda_y \mathbf{K}_5 + \lambda_y^2 \mathbf{K}_4^T + \lambda_x \mathbf{K}_3^T + \lambda_y \mathbf{K}_2^T + \mathbf{K}_1^T \right) \mathbf{v} = \mathbf{0} \tag{2.21}$$

where the matrices $\boldsymbol{K}_i$ are:

$$\mathbf{K}_1 = \begin{bmatrix} \mathbf{0} & \mathbf{0} & \mathbf{d}_{19} \\ \mathbf{0} & \mathbf{0} & \mathbf{d}_{29} \\ \mathbf{0} & \mathbf{0} & \mathbf{d}_{39} \end{bmatrix} \tag{2.22}$$

$$\mathbf{K}_2 = \begin{bmatrix} \mathbf{0} & \mathbf{d}_{16} & \mathbf{d}_{17}+\mathbf{d}_{59} \\ \mathbf{0} & \mathbf{d}_{26} & \mathbf{d}_{27} \\ \mathbf{0} & \mathbf{d}_{36} & \mathbf{d}_{37}+\mathbf{d}_{89} \end{bmatrix} \tag{2.23}$$

$$\mathbf{K}_3 = \begin{bmatrix} \mathbf{d}_{15} & \mathbf{0} & \mathbf{d}_{18} \\ \mathbf{d}_{25} & \mathbf{0} & \mathbf{d}_{28}+\mathbf{d}_{69} \\ \mathbf{d}_{35} & \mathbf{0} & \mathbf{d}_{38}+\mathbf{d}_{79} \end{bmatrix} \tag{2.24}$$

$$\mathbf{K}_4 = \begin{bmatrix} \mathbf{0} & \mathbf{d}_{56} & \mathbf{d}_{57} \\ \mathbf{0} & \mathbf{0} & \mathbf{0} \\ \mathbf{0} & \mathbf{d}_{86} & \mathbf{d}_{87} \end{bmatrix} \tag{2.25}$$

$$\mathbf{K}_5 = \begin{bmatrix} \mathbf{d}_{11}+\mathbf{d}_{55} & \mathbf{d}_{12} & \mathbf{d}_{13}+\mathbf{d}_{58} \\ ... & \mathbf{d}_{22}+\mathbf{d}_{66} & \mathbf{d}_{23}+\mathbf{d}_{67} \\ Symm & ... & \mathbf{d}_{33}+\mathbf{d}_{77}+\mathbf{d}_{88}+\mathbf{d}_{99} \end{bmatrix} \tag{2.26}$$

If the dynamic stiffness matrix $\boldsymbol{D}$ is symmetric, one can show that $\boldsymbol{K}_1 = \boldsymbol{K}_9^T$, $\boldsymbol{K}_2 = \boldsymbol{K}_8^T$, $\boldsymbol{K}_3 = \boldsymbol{K}_7^T$ and $\boldsymbol{K}_4 = \boldsymbol{K}_6^T$. This reduces the above problem to a higher order palindromic generalized eigenvalue problem with multiple variables, which can generally only be solved for some special cases.

We define the following cases:

1.) If $\hat{k}_{n,y} = 0$, let $\lambda_x = \lambda_{0,x}\lambda_n$ where $\lambda_n = e^{i\alpha\hat{k}_{n,x}h_x}$ and solve Eq. (2.21) for λ_n:

$$\left(\lambda_{0,x}^2\lambda_n^2\left(\lambda_y^2\mathbf{K}_1+\lambda_y\mathbf{K}_2+\mathbf{K}_4\right)+\lambda_{0,x}\lambda_n\left(\lambda_y^2\mathbf{K}_3+\lambda_y\mathbf{K}_5+\mathbf{K}_3^T\right)+\lambda_y^2\mathbf{K}_4^T+\lambda_y\mathbf{K}_2^T+\mathbf{K}_1^T\right)\mathbf{v}=\mathbf{0} \tag{2.27}$$

2.) If $\hat{k}_{n,x} = 0$, let $\lambda_y = \lambda_{0,y}\lambda_n$ where $\lambda_n = e^{i\alpha\hat{k}_{n,y}h_y}$ and solve Eq. (2.21) for λ_n:

$$\left(\lambda_{0,y}^2\lambda_n^2\left(\lambda_x^2\mathbf{K}_1+\lambda_x\mathbf{K}_3+\mathbf{K}_4^T\right)+\lambda_{0,y}\lambda_n\left(\lambda_x^2\mathbf{K}_2+\lambda_x\mathbf{K}_5+\mathbf{K}_2^T\right)+\lambda_x^2\mathbf{K}_4^T+\lambda_x\mathbf{K}_3^T+\mathbf{K}_1^T\right)\mathbf{v}=\mathbf{0} \tag{2.28}$$

3.) If $\lambda_x = \lambda_y = \lambda$, Eq. (2.21) becomes:

$$\left(\lambda^4\mathbf{K}_1+\lambda^3\left(\mathbf{K}_2+\mathbf{K}_3\right)+\lambda^2\left(\mathbf{K}_4+\mathbf{K}_5+\mathbf{K}_4^T\right)+\lambda\left(\mathbf{K}_3^T+\mathbf{K}_2^T\right)+\mathbf{K}_1^T\right)\mathbf{v}=\mathbf{0} \tag{2.29}$$

These cases can all be written in the generalized form:

$$\left(\lambda^2\boldsymbol{A}_1^T+\lambda\boldsymbol{A}_0+\boldsymbol{A}_1\right)\boldsymbol{x}=\mathbf{0} \tag{2.30}$$

where $\boldsymbol{A}_0 = \boldsymbol{A}_0^T$. This can for instance be solved by introducing the matrix pencil $Z \pm \lambda Z^T$ [13, 27, 29, 49, 93], with

$$\boldsymbol{Z} = \begin{bmatrix} \boldsymbol{A}_1^T & \boldsymbol{A}_0-\boldsymbol{A}_1 \\ \boldsymbol{A}_1^T & \boldsymbol{A}_1^T \end{bmatrix} \tag{2.31}$$

Several algorithm exists that can efficiently solve this matrix pencil, while preserving the symplectic structure [29, 93]. Examples are QR-like [73], Jacobi-like [27] and a URV-decomposition-based [72] algorithms. Additionally, other linearizations are also proposed that can be solved using methods that are based on Patel's and Arnoldi methods [29].

However, as most of the computational time is spend in the dynamic condensation and not in solving the quadratic eigenvalue problem, a standard eigenvalue solver is used to solve the matrix pencil.

2.4. Transmission

In order to verify the band structure calculations and to get a better understanding of the wave propagation through periodic structures, we can calculate the transmission spectra for several types of imposed harmonic excitations.

We can define the transmission T, in decibels, as the ratio between the magnitudes of the displacements at the point where the response is collected ($||\boldsymbol{U}_o||$) and the point where the structure is excited ($||\boldsymbol{U}_i||$):

$$T(\omega) = 20\log_{10}\left(\frac{||\boldsymbol{U}_o||}{||\boldsymbol{U}_i||}\right) \tag{2.32}$$

Obtaining the transmission could be done in two ways: using a mode superposition approach and using a direct approach. Both have advantages and disadvantages. The mode superposition approach is approximating the system response using mode superposition, with a limited number of eigenmodes. This is typically less computationally intensive if the system response needs to be calculated for many frequencies, as eigenvalue analysis is the most intensive part, which only has to be done once for all frequencies. However, there is some loss of accuracy if too few eigenmodes are used.

On the other hand, if only a limited number for frequencies is required, then the direct approach may be faster. The calculations per frequency are more intensive, as this requires a factorization of the systems of equations for every frequency, however one can skip the intensive eigenvalue analysis that was required for the other approach. Besides, there are no approximations introduced due to the truncation of modes, unlike the mode superposition approach.

In both cases we excite a structure where the PUC is N times periodically repeated in one or two dimensions with a harmonic force $\boldsymbol{F} = \bar{\boldsymbol{F}}\cos\omega t$ and assume a steady state response $\boldsymbol{U} = \frac{A}{2}\boldsymbol{\phi}\cos(\omega t)$ with amplitude A and shape $\boldsymbol{\phi}$.

Differentiating the displacement field twice with respect to time yields $\ddot{\boldsymbol{U}} = -\omega^2\frac{A}{2}\boldsymbol{\phi}\cos(\omega t)$. Substitution of the discretized acceleration, discretized displacements, and periodic force vector into the equations of motion yields the following systems of equations:

$$\left(-\omega^2\boldsymbol{M}+\boldsymbol{K}\right)\frac{A}{2}\boldsymbol{\phi}\cos(\omega t) = \bar{\boldsymbol{F}}\cos\omega t, \tag{2.33}$$

which can be simplified as

$$\left(\boldsymbol{K}-\omega^2\boldsymbol{M}\right)\frac{A}{2}\boldsymbol{\phi} = \bar{\boldsymbol{F}}. \tag{2.34}$$

2.4.1. Direct approach

For the direct approach, we solve the systems of equations from Eq. (2.34) for $\boldsymbol{\phi}$ for every frequency ω and then calculate the corresponding transmission.

2.4.2. Mode superposition approach

For the modal approach, we solve Eq. (2.34) by an eigenmode series expansion. We first compute n eigenmodes $\boldsymbol{\phi}_j$ of the structure and assume that the forced response is a linear combination of the eigenmodes:

$$\boldsymbol{\phi} = \sum_{j=1}^{n}\eta_j\boldsymbol{\phi}_j \tag{2.35}$$

Using the eigenmode orthogonality property and substitution into Eq. (2.34), gives the spectral coordinates:

$$\eta_j = \frac{\boldsymbol{\phi}_j^T\bar{\boldsymbol{F}}}{\left(\omega_j^2-\omega\right)\mu_j}, \tag{2.36}$$

where $\mu_j = \boldsymbol{\phi}_j^T\boldsymbol{M}\boldsymbol{\phi}_j$ is the generalized mass of mode j. We can then obtain an expression for the shape $\boldsymbol{\phi}(\omega)$:

$$\boldsymbol{\phi} = \sum_{j=1}^{n}\frac{\boldsymbol{\phi}_j\boldsymbol{\phi}_j^T}{\left(\omega_j^2-\omega\right)\mu_j}\bar{\boldsymbol{F}} \tag{2.37}$$

This equation can be solved for every ω to obtain the transmission spectra $T(\omega)$.

2.5. Results and discussion

2.5.1. Zig-zag structure analysis

Figure 2.2a shows the real and imaginary components of the band structure for a zig-zag folded strip in the flat configuration ($\theta = 0°$), with non-dimensional parameters $\zeta = 0.1, \gamma = 0.01$, and $\eta = 10^{-3}$. The figure also shows the transmission spectra of waves for excitations in x, y, and z directions for a zig-zag array consisting of 10 unit cells.

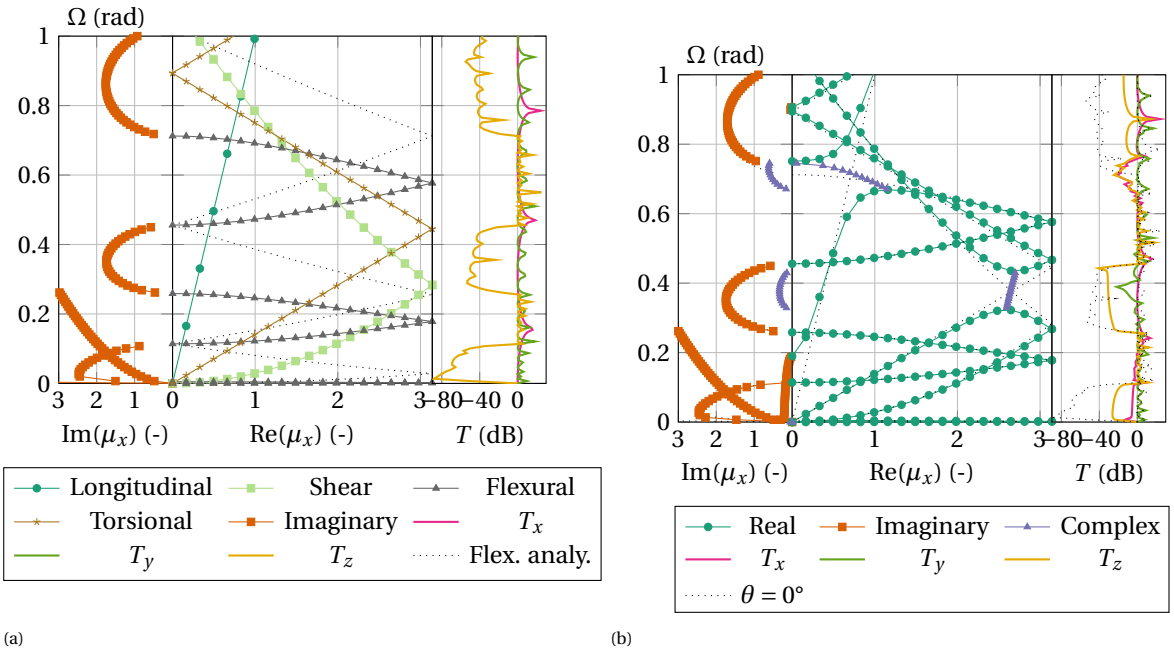

(a) (b)

Figure 2.2: Real (middle) and imaginary (left) components of the band structure and wave transmission spectra (right) for excitations in x,y, and z directions for two configurations of the zig-zag structure. For the transmission spectra plot, a structure with 10 unit cells is used and the transmission in x, y, and z-directions is plotted. (a) shows the structure in the flat configuration ($\theta = 0°$), where the dotted lines are the analytical solutions for flexural wave polarizations, according to Eq. (2.43). (b) is the structure with a small fold angle $\theta = 1.66°$, where the dotted lines are the real and imaginary components in the flat state ($\theta = 0°$).

For the real band structure, several distinct families of bands can be distinguished: longitudinal, shear, flexural and torsional. The analytical solutions for these longitudinal 'L', shear 'S', and flexural 'F' wave polarizations for a flat plate are given by [88].

$$\omega_L(\kappa) = \sqrt{\frac{E}{\rho(1-\nu^2)}}k_x \tag{2.38}$$

$$\omega_S(\kappa) = \sqrt{\frac{E}{2\rho(1+\nu)}}k_x \tag{2.39}$$

$$\omega_F(\kappa) = \sqrt{\frac{D}{t\rho}}k_x^2 \tag{2.40}$$

Which in non-dimensional form are:

$$\Omega_L(\mu_x) = \frac{a}{L_x}\mu_x \tag{2.41}$$

$$\Omega_S(\mu_x) = \frac{a}{L_x}\mu_x\sqrt{\frac{1-\nu^2}{2(1+\nu)}} \tag{2.42}$$

$$\Omega_F(\mu_x) = \frac{\gamma a^2}{\sqrt{12}}\left(\frac{\mu_x}{L_x}\right)^2 \tag{2.43}$$

where $\mu_x = k_x L_x \in [0,\pi]$ is the normalized wave vector.

The numerical solutions for the shear and the longitudinal modes in Fig. 2.2a are in accordance with the analytical solutions (2.41) and (2.42). The flexural bands, however, are not in accordance with the analytical solutions due to the introduction of a crease. The flexural modes become purely imaginary for some frequencies and several modal bandgaps can be seen, where flexural modes are forbidden from propagating through the structure. The size of the imaginary part indicates how much the transmission is damped, as can be seen by comparing the transmission spectra plot from the same figure with the imaginary plot. Only flexural modes can be excited with displacements in pure z direction; all other modes are "deaf" for this excitation. The transmission is therefore largely determined by the imaginary part of the flexural modes.

The families of bands from Fig. 2.2a are uncoupled from the other modes. However, by introducing an out-of-plane component by applying a small fold to the structure, modes may become coupled at their intersection points and a clear distinction between the modes cannot be made anymore. The families of modes start to merge, and modal bandgaps start to form at the centers of the intersections, as can be seen in Fig. 2.2b. In this figure, the band structure and transmission spectra of the zig-zag structure have been plotted for a small fold angle $\theta = 1.66°$.

Comparing the two different dispersion relations from Figs. 2.2a and 2.2b, we can observe a coupling between the longitudinal and the flexural families in two locations: near $\Omega = 0\,\text{rad}$ and $\Omega = 0.7\,\text{rad}$. Near those original intersection points, the modes become respectively imaginary and complex. This is reflected in the transmission plot by the amplitude decay of the waves in x-directions at those frequencies. On the other hand, the transmission in the z-direction shows an increase in magnitude. This is likely because the newly formed coupled-mode also dominates the transmission for excitations in z-direction.

The torsional and shear families of modes show a coupling near $\Omega = 0.4\,\text{rad}$. The two branches are connected through a complex band. As a result, there is a small drop in transmission for the y-direction, which is expected as the now coupled shear mode (which dominates the y-direction) is complex at that location.

It can thus be seen that both the introduction of a crease and an out-of-plane component can lead to interesting wave phenomena in the form of separation of modes and the forming of (modal) bandgaps. If both effects are combined in the right way, it is expected that large complete bandgaps may form in which no waves can propagate through the structure. Applying this knowledge to the Miura-Ori structure may allow us to find complete bandgaps for structures with periodicity in two dimensions as well, where complete bandgaps are typically less commonly found than in their strip counterparts [65, 88].

2.5.2. Miura-Ori structure analysis

Figure 2.3 shows the band structure for a flat Miura-Ori sheet for two different fold stiffnesses: $\eta = \infty$ (no crease) and $\eta = 3$. Within the $\Gamma - X$ and $Y - \Gamma$ segments, one may recognize analytically obtained branches for the flat plate without fold ($\eta = \infty$) from Eqs. (2.41) to (2.43). For the $Y - \Gamma$ segment, the analytical equations are similar, but then with k_y, μ_y and L_y.

It can be seen that by introducing a crease with a difference in bending stiffness ($\eta < \infty$), modal bands start to open up between the flexural modes at several locations, most noteworthy between the fourth and fifth flexural bands. This behavior was also found for the zig-zag structure, where introducing folds also led to modal bandgaps. If, similarly to the zig-zag structure, the shear and longitudinal modes become coupled to (flexural) modes due to out-of-plane components, full complete bandgaps may form between the fourth and fifth band.

When the structure is in the folded configuration, the same behaviour is observed. When a fold is introduced, two flexural eigenmodes will become disconnected at Γ and there is a possibility for a complete band to form. As we will later see, introducing a crease is a necessary condition for a complete bandgap in the dispersion relation to form.

Optimum A

We optimize the various dimensionless design parameters and found two distinct local optima. The first optimum was found by setting $\gamma = 0.01$ and $\eta = 10^{-3}$ and performing a Nelder-Mead optimization for the non-dimensional size between the fourth and the fifth band. A local optimum was found with parameters $\zeta = 0.694\,27$, $\alpha = 55.0°$ and $\theta = 52.86°$; we call this configuration *Optimum A*.

The bandgap occurs between the fourth and fifth bands, which is different from the gap found by Pratapa *et al.* [65], as they found a gap between the eighth and ninth bands. However, as we have seen with the zig-zag structure, the folding of branches is repeated for branches with higher frequencies. It is therefore not unlikely that for certain configurations a band may form between the eighth and ninth bands.

The complete bandgap has been plotted in Fig. B.1. The bandgap is constrained by two points, point (a) and (b) respectively. The deformation modes for these points, which are shown in Fig. 2.5, are in both cases largely determined by out-of-plane vibrations of the panels (perpendicular to the panel planes), while the edges of the panels remain mostly stationary. This is reflected in the band structure by the almost completely horizontal bands, and by the fact that the first natural frequency of the individual panels $\Omega_n = 0.129\,\text{rad}$ is right in the middle of the bandgap.

We may therefore conclude that the bandgap is determined by the local resonance within the unit cells of the structure, which interact with Bragg resonance from the lattice symmetry. The structure has a sub-

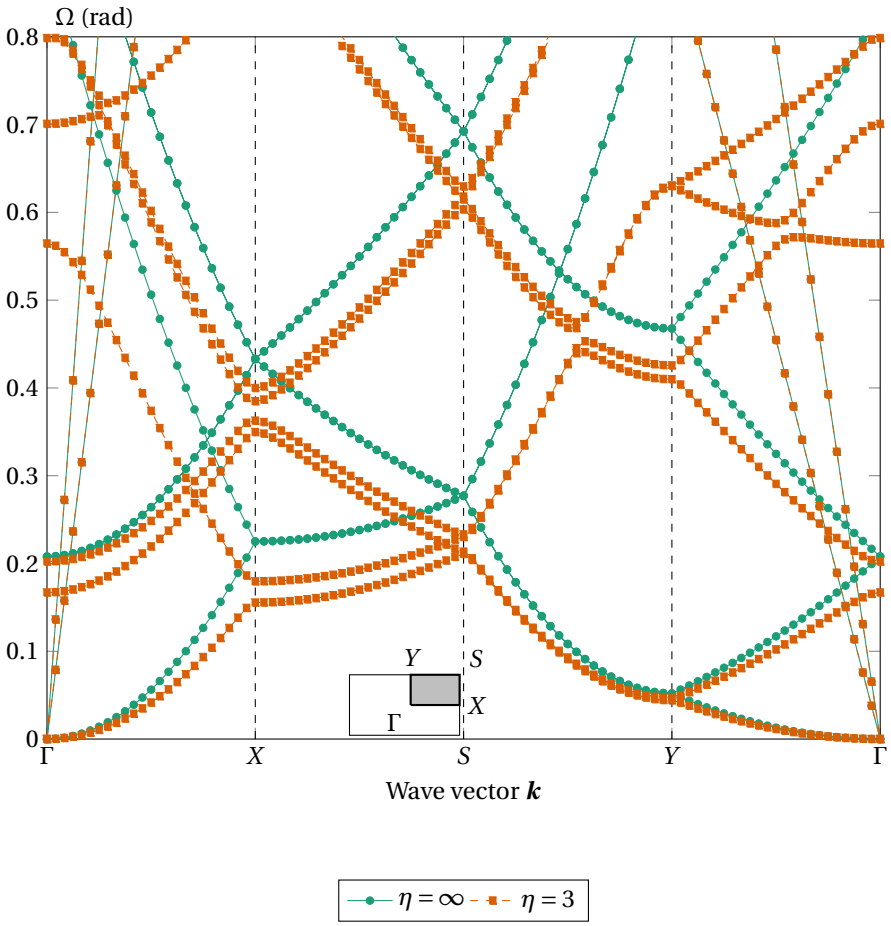

Figure 2.3: Dispersion relation of the optimized Miura-Ori pattern in the flat configuration ($\theta = 0°$) without folds ($\eta = \infty$) and for a stiff fold ($\eta = 3$) along the IBZ. The bands open up between the fourth and fifth flexural mode (starting at $\Omega \approx 0.6$ rad in Γ).

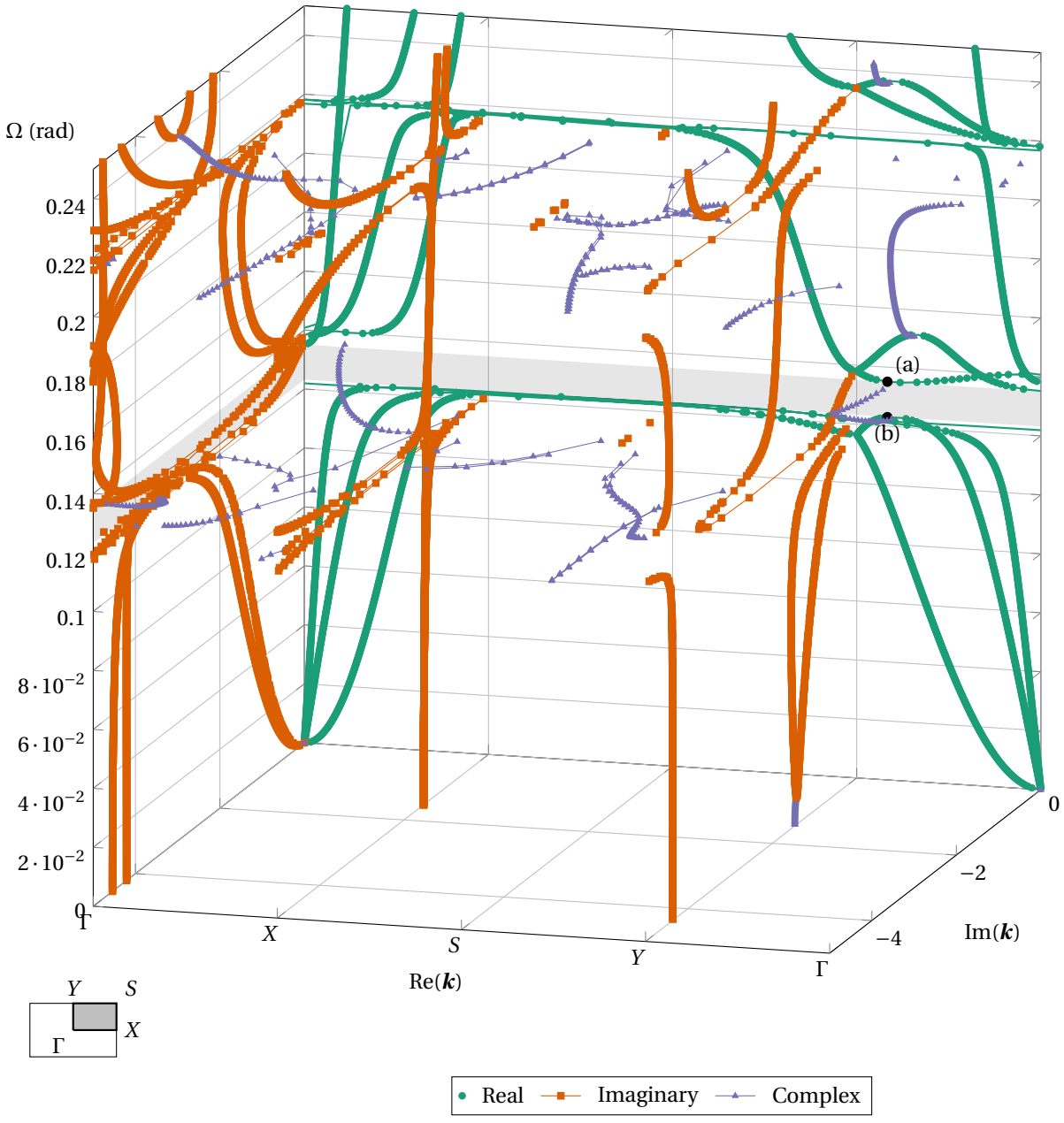

Figure 2.4: The real and imaginary parts of the dispersion relation of the optimized Miura-Ori structure (optimum A). A 2D representation of this 3D figure can be found in Appendix B (Fig. B.1)

wavelength periodicity as the scale of the structure is roughly one order of magnitude smaller than the incident waves.

The modes at points (a) and (b) are connected through a complex mode, which indicates a transfer of symmetry. Looking at the mode shapes, this is indeed the case. These evanescent modes are therefore expected to resemble the mode shapes at (a) and (b), but then exponentially decaying.

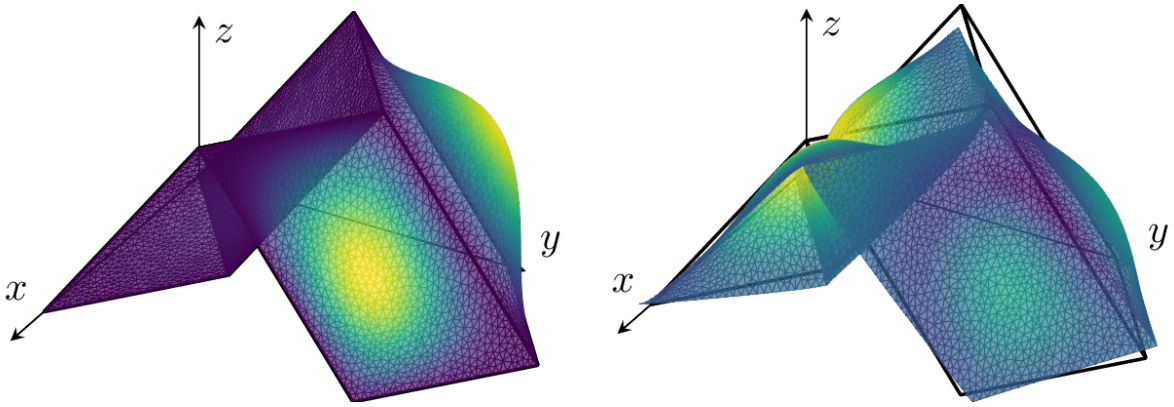

(a) (b)

Figure 2.5: Different mode shapes of the unit cell of the Miura-Ori pattern for optimum A for critical locations in the band structure. Locations of the modes are indicated in Fig. B.1. The colors indicate the magnitude of the displacement. The eigenvectors are complex valued, so the shape at $t = 0$ is shown. The shape of the unit cell in undeformed configuration is indicated with the black outline.

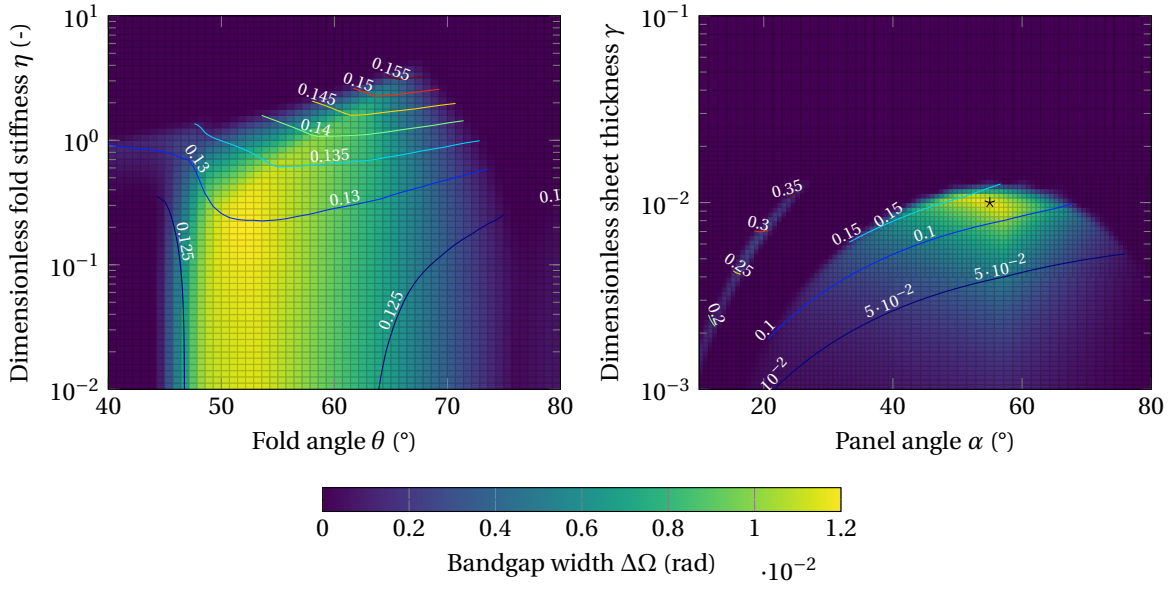

Figure 2.6: The non-dimensional bandgap width and center frequencies, for perturbations of the dimensionless stiffness η and the fold angle θ (left), and the dimensionless thickness γ and the panel angle α (right) of the configuration in Optimum A ($\zeta = 0.69427, \alpha = 55.0°, \gamma = 0.01, \theta = 52.86°, \eta = 0.15848$). The center frequencies (in rad) are indicated with the contour lines. The black star denotes the location of the optimum.

The non-dimensional bandgap width and center frequency has been plotted in Fig. 2.6 for diversions of the design parameters on the local optimum in, respectively, the fold angle θ, crease stiffness η, panel angle α, and the dimensionless sheet thickness γ.

The bandgap width $\Delta\Omega$ is defined as the difference between the maximum value of the fourth band and the minimum value of the fifth band and is zero if this difference is negative. The center frequency is defined as the average of these values and is indicated with contour lines.

As the bandgap width is given in the non-dimensional form, the real size of the gap could be scaled by, for instance, changing the material properties. The argument could be made that by scaling the configuration

with a low center frequency, one could effectively arrive at a larger bandgap at a higher frequency than a configuration that already has a higher center frequency. However, in this study, we are only concerned with the maximum size of the bandgap for a given set of material properties.

The left plot in Fig. 2.6 shows that the structure has a bandgap for a large range of fold angles. The figure also shows that, as expected, a fold with a smaller stiffness is required for a bandgap to form.

The predominant deformation modes that we have seen in Fig. 2.5 may explain why there is a bandgap for a large range of fold angles θ. As the panel deformations are dominant, it effectively does not matter how much the structure is folded.

In the right plot from Fig. 2.6, we can see two regions that have a bandgap: a narrow arc on the left and a wide region on the right. The region on the right shows a bandgap with a small center frequency for a large range of panel angles and sheet thicknesses. On the other hand, the arc on the left shows a bandgap for limited combinations of panel angles and sheet thicknesses, but with a larger center frequency. We will later see that these regions show very distinct deformation characteristics.

Optimum B

The second local optimum was found by choosing a starting point in the narrow arc on the left from Fig. 2.6, and relaxing the constraints for γ and η. We obtain an optimized structure with the following parameters: $\alpha = 65.8013°$, $\theta = 75.5886°$, $\zeta = 0.52687$, $\gamma = 7.3025 \times 10^{-2}$ and $\eta = 2.01786 \times 10^{-3}$. The real and imaginary components of the band structure for this optimum have been plotted in Fig. 2.7.

Comparing the band structure with the previously found optimum, we conclude that this optimum is clearly distinct from the other one. Unlike optimum A, the bandgap center frequency is not determined by the first natural frequency (which is in this case equal to $\Omega_n = 0.162\,\text{rad}$) of the panels, but is much larger. The periodicity of the structure is in this case comparable to the incident wavelength and the sub-wavelength periodicity does not hold anymore. The bandgap is therefore—similar to PnCs—likely due to periodic Bragg scattering and/or Mie scattering [47]. As a consequence, the dynamical behavior is therefore different, which may allow for a more diverse control of wave propagation characteristics that one can achieve with the Miura-Ori pattern.

When comparing the imaginary parts of the first harmonics for both local optima, one may argue that the second local optimum is better suited for vibration isolation, since optimum A has larger imaginary components of the first harmonic inside the bandgap. Evanescent modes for optimum B will therefore likely show a larger decay in amplitude. Optimum B will therefore have better vibration isolation characteristics, even though one could change the material properties such that the width of the bandgap is equal.

Five relevant positions (a - e) have been marked in the band structure. The mode shapes of the Miura-Ori unit cell for these positions are shown in Fig. 2.8. The mode shapes of mode (c) and (d) are similar, whereas the mode shapes of (a) and (b) are not. This can be explained by looking at the imaginary components; (c) and (d) are connected through a complex branch, whereas (a) and (b) are not. Modes that are connected through complex or imaginary branches typically indicate the transfer of symmetry.

As the imaginary part of the branch between (c) and (d) is closest to zero, one can expect an evanescent mode that shares symmetry with the modes in (c) and (d) to be the dominant mode of vibration in the bandgap.

Figure 2.9 shows the size and center frequency of the bandgap as a function of the panel angle α and the dimensionless sheet thickness γ. Comparing this plot with the same plot for optimum A, we can see that the arc on the left has become bigger at the cost of the other region.

Figure 2.9 shows the size and center frequency of the bandgap between the fourth and the fifth bands as a function of the fold angle θ and the dimensionless fold stiffness η for optimum B. Similar to the other optimum, there is only a bandgap for a limited range of fold angles. However, for this optimum, the range is a lot smaller than for the other one. One can also conclude that for a bandgap to appear, there should be a fold at the edges of the panels.

To further illustrate the tunability of the Miura-Ori structure, the complete band structure has been plotted for a selection of fold angles θ in Fig. 2.10. The locations are indicated in Fig. 2.9. In all cases, there are partial bands visible, where the waves with certain frequencies are not able to propagate in both the $\Gamma - X$ and $X - S$ directions. Only for certain fold angles θ, the waves are completely blocked in all directions, including the $S - Y$ and $Y - \Gamma$ directions.

By folding the structure, one can thus both control the direction of prorogation as well as the attenuation of waves within a certain frequency range. This can be done after the structure is produced, which is a great advantage over the traditional metamaterials and may open up new applications for acoustic metamaterials.

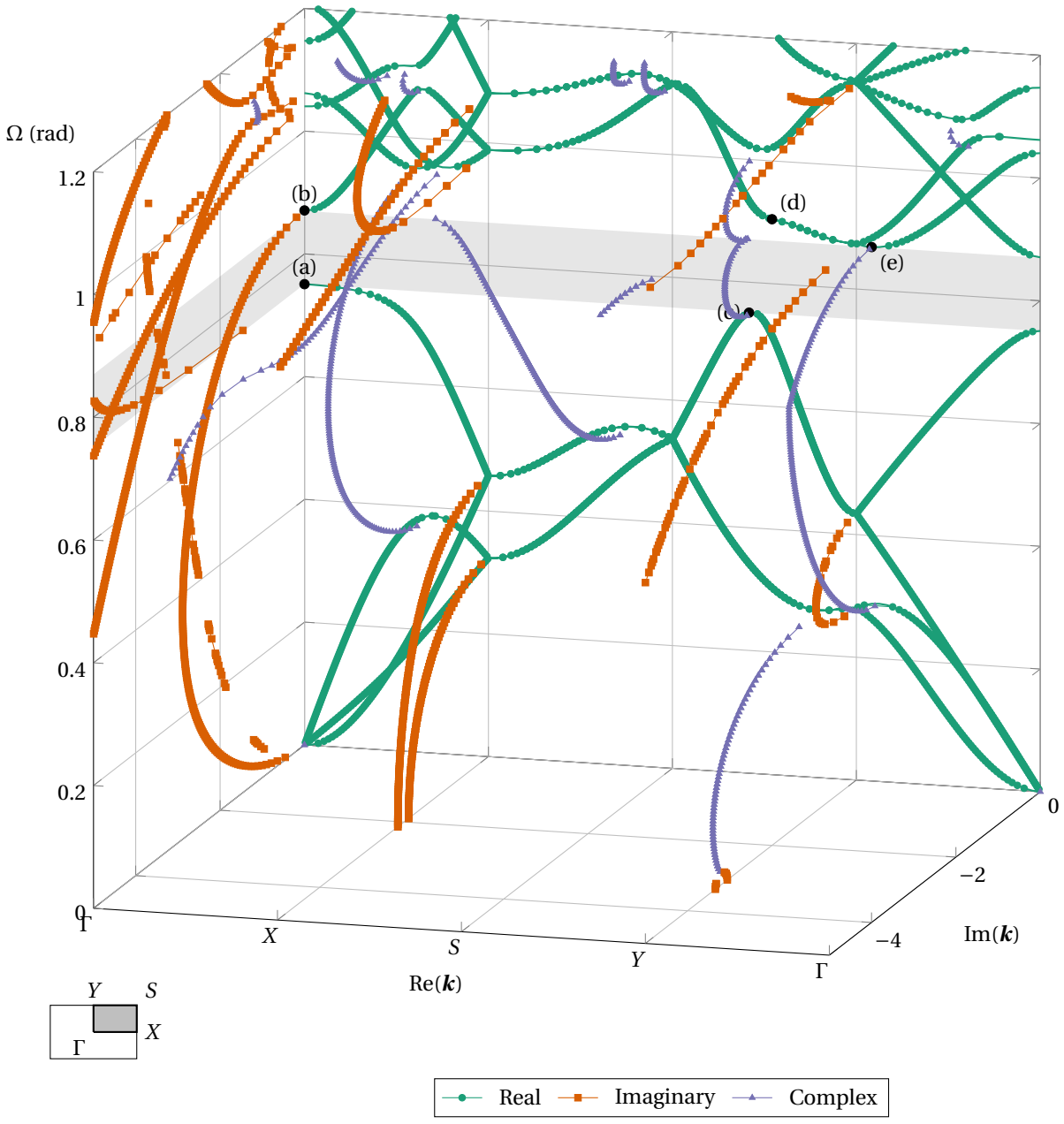

Figure 2.7: The real and imaginary parts of the dispersion relation of the optimized Miura-Ori structure (optimum B). A 2D representation of this 3D figure can be found in Appendix B (Fig. B.2)

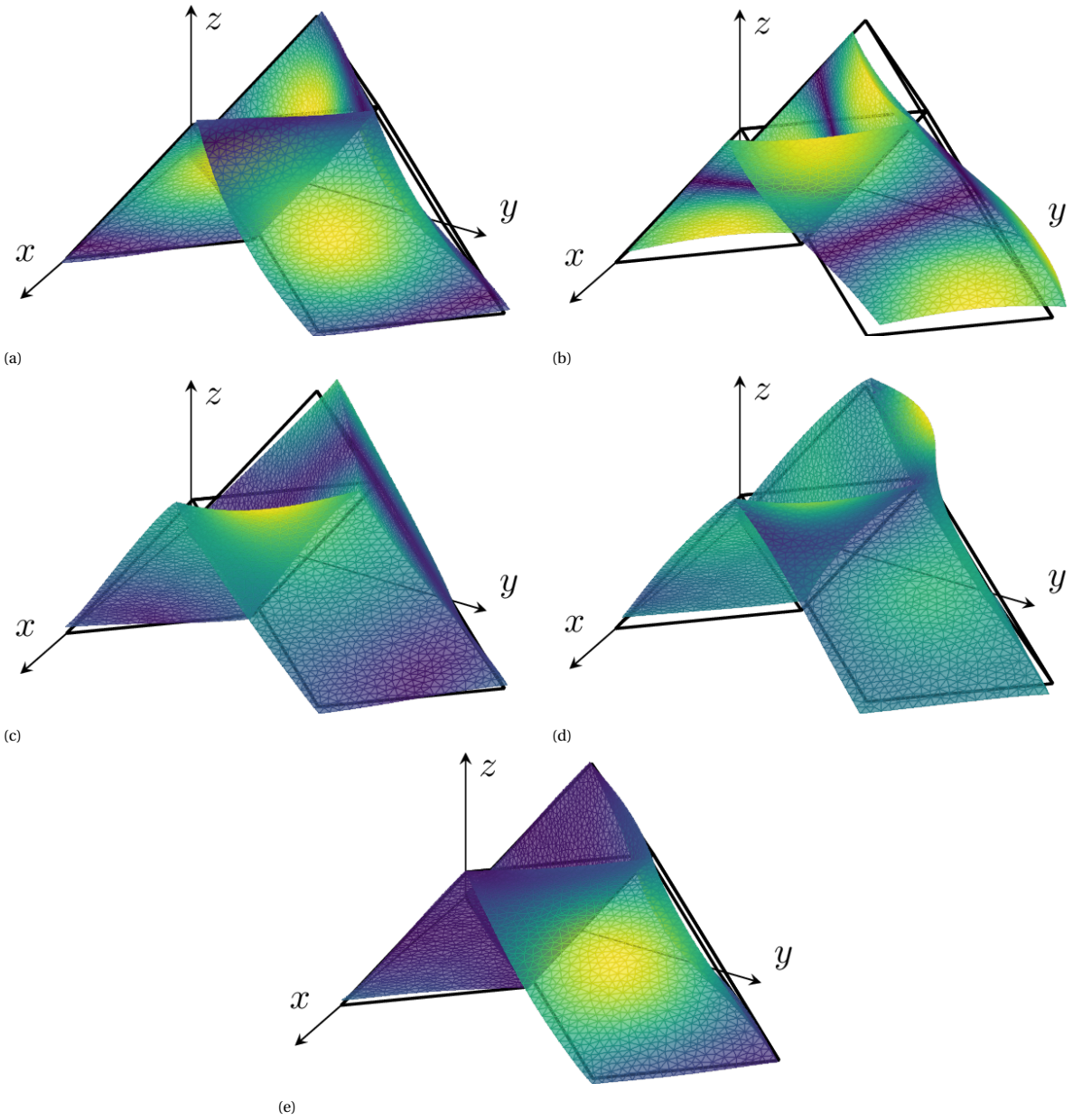

Figure 2.8: Different mode shapes of the unit cell of the Miura-Ori pattern for optimum B for critical locations in the band structure. Locations of the modes are indicated in Fig. B.2. The colors indicate the magnitude of the displacement. In Figs. 2.8c to 2.8e, the eigenvectors are complex valued, so the shape at $t = 0$ is shown. The shape of the unit cell in undeformed configuration is indicated with the black outline.

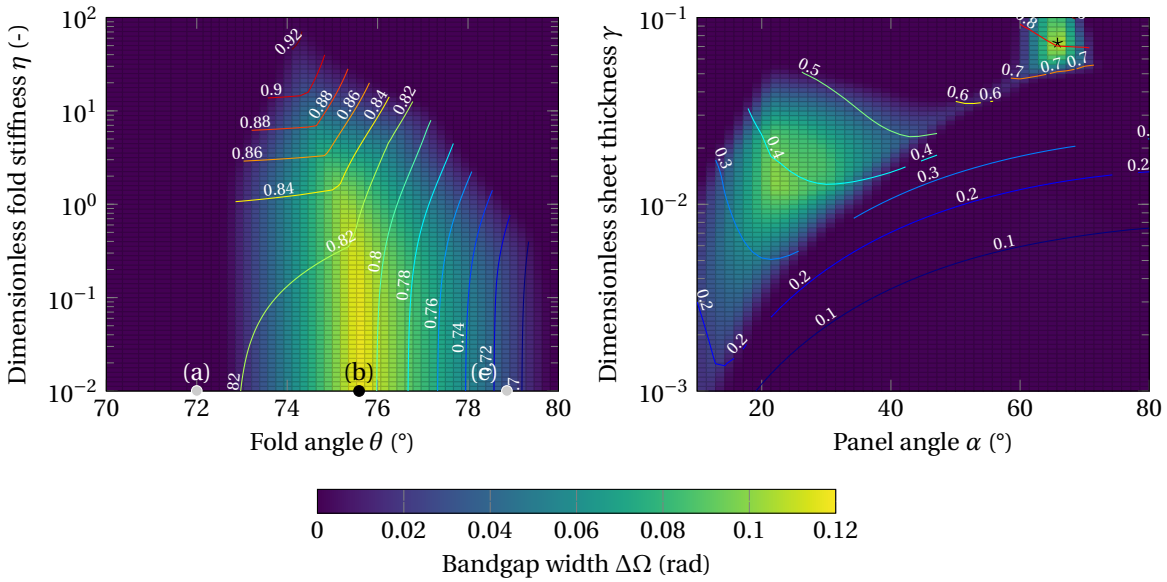

Figure 2.9: The non-dimensional bandgap width and center frequencies, for perturbations of the dimensionless stiffness η and the fold angle θ (left), and the dimensionless thickness γ and the panel angle α (right) of the configuration in Optimum B ($\zeta = 0.52687, \alpha = 65.8°, \gamma = 7.3025 \times 10^{-2}, \theta = 75.59°, \eta = 2.01786 \times 10^{-3}$). The center frequencies (in rad) are indicated with the contour lines and are also shown for small negative bandgap sizes. Points (a), (b) and (c) indicate the locations of the band structures shown in Fig. 2.10. The black star denotes the location of the optimum.

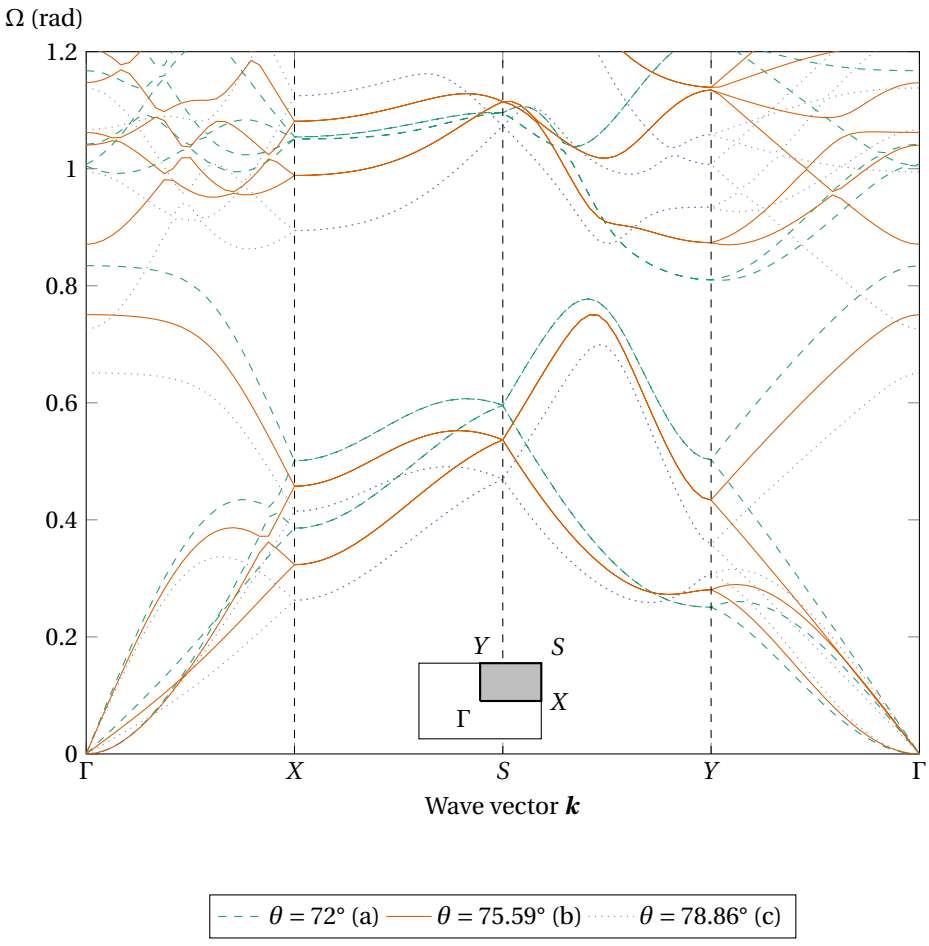

Figure 2.10: Band structure of the optimized Miura-Ori pattern for three fold angles θ for optimum B, locations are indicated in Fig. 2.9. Partial bands exists in all cases.

2.6. Conclusion

In this paper, we have seen that folded sheets (origami) can be used for the active control or tuning of wave propagation through sheets. Due to a combination of an out-of-plane component with a crease, which is more compliant in bending, a (modal) bandgap appears between the fourth and fifth band of the Miura-Ori structure.

The geometrical and material properties of the Miura-Ori sheet determine the location and size of the bandgap and the vibration attenuation characteristics inside the gap, which could be programmed (before manufacturing) or tuned (after manufacturing).

By programming the geometrical properties of the Miura-Ori sheet, one could either create a structure with a periodicity of the same order or an order of magnitude smaller than the wavelength at the gap. In other words, one could either create a phononic crystal or an acoustic metamaterial.

By the simple act of folding one can tune the band structure and thereby, control both the direction of propagation and attenuation of waves for certain ranges of frequencies. As the active control typically cannot be done with traditional structures, it would open up new applications where tunable vibration isolation is desired.

Additionally, the finite element method that was used in this paper can, unlike bar and hinge models, be used for any type of panel. The methods presented in this paper can therefore be used for the analysis of virtually endless types of origami structures that can be used for active vibration isolation.

3

Recommendations

Some parts of the thesis can be improved or investigated deeper, these are listed in this chapter. Reading this chapter might give a direction for future research. The recommendations are:

- An initial goal was to investigate the geometrical non-linear behavior of an origami structure. One may imagine that when larger amplitudes are introduced, it can have a softening or hardening behavior, which may be different for various geometrical configurations. Knowing this would then give a better insight into the filtering properties for waves with larger amplitudes. This is useful for all kinds of applications as unwanted vibrations are typically not small because if these are small, there is typically no need to filter them. Unfortunately, the work on this part was not finished during the project, and further research needs to be conducted.

- For the zig-zag structure, a transmission spectrum is calculated for a strip with 10 unit cells. It would have been interesting to do the same for the Miura-Ori sheet. However, this is computationally intensive, due to the large amounts of DOFs. One may therefore opt to perform this study on a smaller structure, for instance, a sheet with 6x6 unit cells. Alternatively, one may use some kind of Model Order Reduction (MOR) technique to reduce the size of the problem.

- In this study, only numerical results have been obtained; the results are only verified, but not validated. Performing experiments to validate the models is therefore desired. With experiments, one cannot obtain a band structure, since for the band structure an infinite periodic solid is assumed. However, it is possible to obtain a frequency response analysis by, for instance, imposing a harmonic excitation at one end and measuring the displacement at the other end. This could then be compared to the numerically obtained transmission spectra to see whether the numerical results make sense. A possible experimentation setup was described by Trainiti *et al.* [88] for a undulated strip. A similar setup could be used for a zig-zag strip or a Miura-Ori sheet.

- A possible direction for future research is the search for band gaps between higher modes for the Miura-Ori structure. In this study, only a gap was found between the fourth and fifth modes. However, also between higher modes, a bandgap may form, for instance, between the eighth and ninth modes. A more diverse control of waves may then be achieved, if this gap appears at another fold angle or when two or more gaps are present for the same configuration. The study by Pratapa *et al.* [65] already found band gaps between higher modes for the Miura-Ori and Eggbox structures, however, as this study uses a bar and hinge model, the gaps may be different.

- Another possible direction for future research is into other origami patterns that exhibit a bandgap behavior. One could for instance study already known patterns, for instance, the Eggbox structure, and see whether those have a bandgap. Alternatively, one could systemically create new 4-vertex sheets by combining several 4-vertex unit cells into a jigsaw puzzle (see Section 1.1.2), and then optimize the design variables of this puzzle similarly as has been done in this study. Patterns should not have to be limited to sheets as the methods presented in this paper could also be used for origami tubes.

- Both of the previous recommendations rely on finding and optimizing a bandgap. The initial bandgap for the Miura-Ori was found by trial and error, however, this is arguably not the best approach. A better approach would have been to come up with an algorithm that uses the band structure itself to find and optimize the gap. An algorithm that uses the information on how the different lines move through the band structure upon changing the design variables, would probably do a better job optimizing the structure than the currently used algorithm that only takes the size of the gap into account. Especially when an initial bandgap is not yet found.
- A final possible direction for future research is into the complex components of the band structures. These may give valuable new insights into the vibration attenuation characteristics inside the bandgap, but also for specific modes outside the gap. Knowing how different modes are attenuated may give even more control over the wave propagation characteristics.

4

Reflection

This chapter contains a reflection on the progress of the work. It starts with a reflection on the timeline, which is then followed by a more personal reflection. This contains the most important things that were learned during the project. Both sections also contain some points of improvement. Reading this chapter will give the reader hopefully a better understanding of the thesis project as a whole.

4.1. Reflection on the timeline

The project officially started on 1st September 2019, with a literature survey on the topic. Due to personal circumstances and the beginning of the Covid-19 crisis, the literature study was presented at the end of March. In the meantime, I already started working on the second part.

The second part involved modifying the existing code for plate and shell elements and gathering the results for the origami structures. This involved the coding itself and a careful comparison of the results with simple analytical problems or with results from the literature. There were already some studies performed on folded beams and sheets, however, the results did not match those results. First, it was concluded that there must be something wrong with the code, however, there were some other studies on (undulated) plates, where the obtained results did match the results from those studies. It was then concluded that the results were different due to the use of different models, as the folded beams and sheet studies used bar and hinge approaches.

Several geometrical parameters of the Miura-Ori pattern were then varied to find a bandgap in the Miura-Ori pattern. Finding an initial design that has a bandgap in the dispersion relation, proved to be difficult, as there were a lot of design parameters that could be changed. Besides, the configuration that was used by Pratapa *et. al* [65] did not yield a bandgap when using the finite element model. Eventually, a design was found, which was then used as a starting point for the optimization.

The size of the bandgap was then calculated for variations on the optimized design. This was a time-consuming process, as the calculation of the band structure was computationally intensive. An attempt was therefore made to make the code more efficient, and the optimized code was then executed on the cluster.

Additional pieces of code were written to obtain the complex components of the wave vector. The results were compared with the band structure obtained with the previous method, results from the literature, and by obtaining the transmission spectra for a problem where the unit cell was periodically repeated.

It was then decided to continue with investigating geometrical non-linear behaviors, as it was expected that this may have a major influence on the dynamical behavior. A small literature study was performed, as this was initially not included in the original literature survey. It was found that a perturbation approach would be the best method for obtaining a non-linear band structure, as it is impossible to use a fully non-linear method in Fourier domain. The perturbation approach was then implemented in the already existing code. As this method resembles the linear one, only a few additional pieces of code were required. Details for nonlinear band structures and the perturbation approach can be found in Appendix A.

However, this method only works for weak linear problems and does not fully describe the non-linear behavior. Besides, validation of this method proved to be difficult. This had never been done in other literature for similar problems. Comparing results with results from other literature was therefore not possible. To overcome these issues and to check whether there was any effect of geometrical nonlinearities at all, we

decided to perform time-domain simulations of a structure with several repeated unit cells and obtaining the transmission for several imposed excitation amplitudes. First, non-linear transient time-domain simulations using Newmark's method were tried, however, these proved to be unstable for larger amplitude and time. Then, another time-domain method was used, namely Bathe's method. This method was more stable than Newmark's method, as it would give seemingly accurate results for amplitudes in the linear regime. However, it faced the same stability issues for slightly larger amplitudes.

At this time in the project, too much time had been spent on the non-linearities, without any good results. It was uncertain how much extra time it would take. And as it is at some point time to wrap up, it was unfortunately decided to drop the research into non-linear behavior and finish the thesis with only the linear dynamical behavior.

In hindsight, it would have been better to stop earlier. However, I wanted to finish it as I had the feeling that I was becoming closer. A point of improvement would therefore be to take a step back sometimes, analyze how much time it would take extra, and see whether it is really necessary. I think I sometimes lost a bit of the overview on the planning and on the things that needed to be done.

The last part of the thesis was then devoted to writing the paper and report. Although some parts were already written down in an earlier stage, a lot of writing still had to be done. As my supervisor said: "do not leave the writing until the end". This is what I partially did, but it still could have been better.

4.2. Personal reflection

Working on a thesis requires a lot of self-discipline, as it is an individual project and there are not a lot of deadlines. As a consequence, you would have to plan and organize the work yourself. Especially at the beginning of the thesis, I found it challenging to make progress. Luckily the guidance of my supervisor helped. His enthusiasm and involvement motivated me a lot to make progress. As the project continued, there were periods where I made a lot of progress, which extra motivated me to continue. However, there were also periods where I got stuck, and whereas a consequence motivation was a bit lacking. Nevertheless, by simply continuing working you will eventually make progress with little steps at a time. In the end, I think that having gone through these periods was good for my personal development.

Previously, I had already some experience with coding in Python, which helped a lot at the beginning of the thesis. It is easier to understand the structure of the code if you already know the language. However, I have still improved my programming skills during the thesis by spending a lot of time writing, improving, and debugging pieces of code. The key thing to remember here is to start simple and test each separate part of the code. At first, this seemed a bit waste of time to me, but I've later learned that the opposite is true.

Also in terms of the content of the study I have learned a lot. During the literature study phase, I remember that I had a hard time understanding several topics. However, if I now look back at those topics, it all seems rather simple. On the one hand, this demonstrates the learning path I took to understand the topics. But on the other hand, it is a bit disappointing that I have to stop here, as there is so much more to learn.

Overall, I found the thesis an enriching experience. It has broadened my knowledge on, for instance, the finite element method, acoustic metamaterials, phononic crystals, and the dynamical behavior of periodic structures. I have also learned to research at an academic level. And I have learned to tackle problems step by step. All of these are skills and knowledge which I can use in my future career.

Bibliography

[1] Muralidhar Ambati, Nicholas Fang, Cheng Sun, and Xiang Zhang. Surface resonant states and superlensing in acoustic metamaterials. *Physical Review B - Condensed Matter and Materials Physics*, 75(19), 2007. ISSN 10980121. doi: 10.1103/PhysRevB.75.195447.

[2] Waldemar Axmann and Peter Kuchment. An Efficient Finite Element Method for Computing Spectra of Photonic and Acoustic Band-Gap Materials. *Journal of Computational Physics*, 150(2):468–481, 1999. ISSN 00219991. doi: 10.1006/jcph.1999.6188.

[3] Emanuele Baravelli and Massimo Ruzzene. Internally resonating lattices for bandgap generation and low-frequency vibration control. *Journal of Sound and Vibration*, 332(25):6562–6579, dec 2013. ISSN 0022-460X. doi: 10.1016/J.JSV.2013.08.014. URL https://www.sciencedirect.com/science/article/pii/S0022460X13006792.

[4] Maxime Bavencoffe, Bruno Morvan, Jean Louis Izbicki, and Anne Christine Hladky-Hennion. Characterization of evanescent ultrasonic waves in a band gap of a 1D phononic crystal. In *Proceedings - IEEE Ultrasonics Symposium*, pages 1024–1027, Rome, 2009. IEEE. ISBN 9781424443895. doi: 10.1109/ULTSYM.2009.5441893.

[5] S. Biwa, S. Yamamoto, F. Kobayashi, and N. Ohno. Computational multiple scattering analysis for shear wave propagation in unidirectional composites. *International Journal of Solids and Structures*, 41(2):435–457, jan 2004. ISSN 0020-7683. doi: 10.1016/J.IJSOLSTR.2003.09.015. URL https://www.sciencedirect.com/science/article/pii/S002076830300516X.

[6] Felix Bloch. Über die Quantenmechanik der Elektronen in Kristallgittern. *Zeitschrift für Physik*, 52 (7):555–600, jul 1929. ISSN 0044-3328. doi: 10.1007/BF01339455. URL https://doi.org/10.1007/BF01339455.

[7] Elisa Boatti, Nikolaos Vasios, and Katia Bertoldi. Origami Metamaterials for Tunable Thermal Expansion. *Advanced Materials*, 29(26):1–6, 2017. ISSN 15214095. doi: 10.1002/adma.201700360.

[8] V. Brunck, F. Lechenault, A. Reid, and M. Adda-Bedia. Elastic theory of origami-based metamaterials. *Physical Review E*, 93(3):1–14, 2016. ISSN 24700053. doi: 10.1103/PhysRevE.93.033005.

[9] D. Caballero, J. Sánchez-Dehesa, C. Rubio, R. Mártinez-Sala, J. V. Sánchez-Pérez, F. Meseguer, and J. Llinares. Large two-dimensional sonic band gaps. *Physical Review E - Statistical Physics, Plasmas, Fluids, and Related Interdisciplinary Topics*, 60(6):R6316–R6319, 1999. ISSN 1063651X. doi: 10.1103/PhysRevE.60.R6316.

[10] Yongjun Cao, Zhilin Hou, and Youyan Liu. Finite difference time domain method for band-structure calculations of two-dimensional phononic crystals. *Solid State Communications*, 132(8):539–543, nov 2004. ISSN 0038-1098. doi: 10.1016/J.SSC.2004.09.003. URL https://www.sciencedirect.com/science/article/pii/S0038109804007690.

[11] Huanyang Chen and C. T. Chan. Acoustic cloaking in three dimensions using acoustic metamaterials. *Applied Physics Letters*, 91(18):1–4, 2007. ISSN 00036951. doi: 10.1063/1.2803315.

[12] Jiu Jiu Chen, Bernard Bonello, and Zhi Lin Hou. Plate-mode waves in phononic crystal thin slabs: Mode conversion. *Physical Review E - Statistical, Nonlinear, and Soft Matter Physics*, 78(3):1–5, 2008. ISSN 15393755. doi: 10.1103/PhysRevE.78.036609.

[13] Eric King Wah Chu, Tsung Min Hwang, Wen Wei Lin, and Chin Tien Wu. Vibration of fast trains, palindromic eigenvalue problems and structure-preserving doubling algorithms. *Journal of Computational and Applied Mathematics*, 219(1):237–252, 2008. ISSN 03770427. doi: 10.1016/j.cam.2007.07.016.

[14] C. Daraio, V. F. Nesterenko, E. B. Herbold, and S. Jin. Tunability of solitary wave properties in one-dimensional strongly nonlinear phononic crystals. *Physical Review E - Statistical, Nonlinear, and Soft Matter Physics*, 73(2):1–10, 2006. ISSN 15393755. doi: 10.1103/PhysRevE.73.026610.

[15] Erik D. Demaine, Martin L. Demaine, Vi Hart, Gregory N. Price, and Tomohiro Tachi. (Non)Existence of Pleated Folds: How Paper Folds Between Creases. *Graphs and Combinatorics*, 27(3):377–397, 2011. ISSN 09110119. doi: 10.1007/s00373-011-1025-2.

[16] Peter Dieleman, Niek Vasmel, Scott Waitukaitis, and Martin van Hecke. Jigsaw puzzle design of pluripotent origami. *Nature Physics*, 16(1):63–68, 2020. ISSN 17452481. doi: 10.1038/s41567-019-0677-3. URL http://dx.doi.org/10.1038/s41567-019-0677-3.

[17] David C Dobson. An Efficient Method for Band Structure Calculations in 2D Photonic Crystals. *Journal of Computational Physics*, 149(2):363–376, mar 1999. ISSN 0021-9991. doi: 10.1006/JCPH.1998.6157. URL https://www.sciencedirect.com/science/article/pii/S0021999198961575.

[18] D. Duhamel, B. R. Mace, and M. J. Brennan. Finite element analysis of the vibrations of waveguides and periodic structures. *Journal of Sound and Vibration*, 294(1-2):205–220, 2006. ISSN 10958568. doi: 10.1016/j.jsv.2005.11.014.

[19] E N Economou and M M Sigalas. Classical wave propagation in periodic structures: Cermet versus network topology. *Phys. Rev. B*, 48(18):13434–13438, nov 1993. doi: 10.1103/PhysRevB.48.13434. URL https://link.aps.org/doi/10.1103/PhysRevB.48.13434.

[20] E. T. Filipov, G. H. Paulino, and T. Tachi. Origami tubes with reconfigurable polygonal cross-sections. *Proceedings of the Royal Society A: Mathematical, Physical and Engineering Sciences*, 472(2185), 2016. ISSN 14712946. doi: 10.1098/rspa.2015.0607.

[21] E. T. Filipov, K. Liu, T. Tachi, M. Schenk, and G. H. Paulino. Bar and hinge models for scalable analysis of origami. *International Journal of Solids and Structures*, 124:26–45, 2017. ISSN 00207683. doi: 10.1016/j.ijsolstr.2017.05.028.

[22] G. Floquet. Sur les équations différentielles linéaires à coefficients périodiques. *Annales scientifiques de l'École normale supérieure*, 12:47–88, 1883. ISSN 0012-9593. doi: 10.24033/asens.220.

[23] André Foehr, Osama R. Bilal, Sebastian D. Huber, and Chiara Daraio. Spiral-Based Phononic Plates: From Wave Beaming to Topological Insulators. *Physical Review Letters*, 120(20):1–5, 2018. ISSN 10797114. doi: 10.1103/PhysRevLett.120.205501.

[24] Kazuko Fuchi and Alejandro R. Diaz. Origami design by topology optimization. *Journal of Mechanical Design, Transactions of the ASME*, 135(11):1–7, 2013. ISSN 10500472. doi: 10.1115/1.4025384.

[25] R. Ganesh and S. Gonella. From modal mixing to tunable functional switches in nonlinear phononic crystals. *Physical Review Letters*, 114(5):1–5, 2015. ISSN 10797114. doi: 10.1103/PhysRevLett.114.054302.

[26] Saeid Hedayatrasa, Kazem Abhary, M. S. Uddin, and James K. Guest. Optimal design of tunable phononic bandgap plates under equibiaxial stretch. *Smart Materials and Structures*, 25(5), 2016. ISSN 1361665X. doi: 10.1088/0964-1726/25/5/055025.

[27] A. Hilliges, C. Mehl, and V. Mehrmann. On the solution of palindromic eigenvalue problems. *ECCOMAS 2004 - European Congress on Computational Methods in Applied Sciences and Engineering*, (January 2004), 2004.

[28] Yoyo Hinuma, Giovanni Pizzi, Yu Kumagai, Fumiyasu Oba, and Isao Tanaka. Band structure diagram paths based on crystallography. *Computational Materials Science*, 128:140–184, feb 2017. ISSN 0927-0256. doi: 10.1016/J.COMMATSCI.2016.10.015. URL https://www.sciencedirect.com/science/article/pii/S0927025616305110?via{%}3Dihub.

[29] Tsung-Ming Huang, Wei-Wei Lin, and Jiang Qian. Structure-preserving algorithms for palindromic quadratic eigenvalue problems arising from vibration of fast trains. *SIAM Journal on Matrix Analysis and Applications*, 30(4):1566–1592, 2008. doi: 10.1137/080713550.

[30] Mahmoud I. Hussein, Michael J. Leamy, and Massimo Ruzzene. Dynamics of phononic materials and structures: Historical origins, recent progress, and future outlook. *Applied Mechanics Reviews*, 66(4): 1–38, 2014. ISSN 00036900. doi: 10.1115/1.4026911.

[31] Pingting Jiang, Tianxi Jiang, and Qingbo He. Origami-based adjustable sound-absorbing metamaterial. *Smart Materials and Structures*, pages 0–5, mar 2021. ISSN 0964-1726. doi: 10.1088/1361-665X/abf420. URL https://iopscience.iop.org/article/10.1088/1361-665X/abf420.

[32] Charles Kittel. *Introduction to Solid State Physics*. Eight edit edition, 2005. ISBN 978-0-471-41526-8.

[33] F. Kobayashi, S. Biwa, and N. Ohno. Wave transmission characteristics in periodic media of finite length: multilayers and fiber arrays. *International Journal of Solids and Structures*, 41(26):7361–7375, dec 2004. ISSN 0020-7683. doi: 10.1016/J.IJSOLSTR.2004.06.017. URL https://www.sciencedirect.com/science/article/pii/S0020768304003270.

[34] W Kohn and N Rostoker. Solution of the Schrödinger Equation in Periodic Lattices with an Application to Metallic Lithium. *Phys. Rev.*, 94(5):1111–1120, jun 1954. doi: 10.1103/PhysRev.94.1111. URL https://link.aps.org/doi/10.1103/PhysRev.94.1111.

[35] J Korringa. On the calculation of the energy of a Bloch wave in a metal. *Physica*, 13(6-7):392–400, aug 1947. ISSN 0031-8914. doi: 10.1016/0031-8914(47)90013-X. URL https://www.sciencedirect.com/science/article/pii/003189144790013X?via{%}3Dihub.

[36] M S Kushwaha, P Halevi, L Dobrzynski, and B Djafari-Rouhani. Acoustic band structure of periodic elastic composites. *Phys. Rev. Lett.*, 71(13):2022–2025, sep 1993. doi: 10.1103/PhysRevLett.71.2022. URL https://link.aps.org/doi/10.1103/PhysRevLett.71.2022.

[37] M S Kushwaha, P Halevi, G Martinez, L Dobrzynski, and B Djafari-Rouhani. Theory of acoustic band structure of periodic elastic composites. *Phys. Rev. B*, 49(4):2313–2322, jan 1994. doi: 10.1103/PhysRevB.49.2313. URL https://link.aps.org/doi/10.1103/PhysRevB.49.2313.

[38] R J Lang. *Origami Design Secrets: Mathematical Methods for an Ancient Art, Second Edition*. Taylor & Francis, 2nd editio edition, 2011. ISBN 9781568814360. URL https://books.google.nl/books?id=6bhEatkCuWgC.

[39] Vincent Laude, Mikaël Wilm, Sarah Benchabane, and Abdelkrim Khelif. Full band gap for surface acoustic waves in a piezoelectric phononic crystal. *Physical Review E*, 71(3), mar 2005. ISSN 1539-3755. doi: 10.1103/PhysRevE.71.036607. URL https://link.aps.org/doi/10.1103/PhysRevE.71.036607.

[40] Vincent Laude, Younes Achaoui, Sarah Benchabane, and Abdelkrim Khelif. Evanescent Bloch waves and the complex band structure of phononic crystals. *Physical Review B - Condensed Matter and Materials Physics*, 80(9):1–4, 2009. ISSN 10980121. doi: 10.1103/PhysRevB.80.092301.

[41] Arthur Lebée. From folds to structures, a review. *International Journal of Space Structures*, 30(2):55–74, 2015. ISSN 20598033. doi: 10.1260/0266-3511.30.2.55.

[42] F. Lechenault, B. Thiria, and M. Adda-Bedia. Mechanical response of a creased sheet. *Physical Review Letters*, 112(24):1–5, 2014. ISSN 10797114. doi: 10.1103/PhysRevLett.112.244301.

[43] Suyi Li, Hongbin Fang, Sahand Sadeghi, Priyanka Bhovad, and Kon Well Wang. Architected Origami Materials: How Folding Creates Sophisticated Mechanical Properties. *Advanced Materials*, 31(5), feb 2019. ISSN 15214095. doi: 10.1002/adma.201805282.

[44] Sicong Liu, Guoxing Lu, Yan Chen, and Yew Wei Leong. Deformation of the Miura-ori patterned sheet. *International Journal of Mechanical Sciences*, 99:130–142, aug 2015. ISSN 0020-7403. doi: 10.1016/J.IJMECSCI.2015.05.009. URL https://www.sciencedirect.com/science/article/pii/S0020740315001897.

[45] Zhengyou Liu, Xixiang Zhang, Yiwei Mao, Y Y Zhu, Zhiyu Yang, C T Chan, and Ping Sheng. Locally Resonant Sonic Materials. *Science*, 289(5485), sep 2000. doi: 10.1126/science.289.5485.1734. URL http://science.sciencemag.org/content/289/5485/1734.abstract.

[46] Zhengyou Liu, C. T. Chan, and Ping Sheng. Three-component elastic wave band-gap material. *Physical Review B*, 65(16):165116, apr 2002. ISSN 0163-1829. doi: 10.1103/PhysRevB.65.165116. URL https://link.aps.org/doi/10.1103/PhysRevB.65.165116.

[47] Ming-Hui Lu, Liang Feng, and Yan-Feng Chen. Phononic crystals and acoustic metamaterials. *Materials Today*, 12(12):34–42, dec 2009. ISSN 1369-7021. doi: 10.1016/S1369-7021(09)70315-3. URL https://www.sciencedirect.com/science/article/pii/S1369702109703153{#}fig3.

[48] Brian R. Mace and Elisabetta Manconi. Modelling wave propagation in two-dimensional structures using finite element analysis. *Journal of Sound and Vibration*, 318(4-5):884–902, 2008. ISSN 10958568. doi: 10.1016/j.jsv.2008.04.039.

[49] D. Steven Mackey, Niloufer Mackey, Christian Mehl, and Volker Mehrmann. Structured Polynomial eigenvalue problems: Good Vibrations from Good Linearizations. *SIAM Journal on Matrix Analysis and Applications*, 48(4):1029–1051, 2006.

[50] Kevin Manktelow, Raj K. Narisetti, Michael J. Leamy, and Massimo Ruzzene. Finite-element based perturbation analysis of wave propagation in nonlinear periodic structures. *Mechanical Systems and Signal Processing*, 39(1-2):32–46, 2013. ISSN 08883270. doi: 10.1016/j.ymssp.2012.04.015. URL http://dx.doi.org/10.1016/j.ymssp.2012.04.015.

[51] Koen M. Markestein. *Finite element based analysis and validation for nonlinear structural dynamics*. PhD thesis, Delft University of Technology, 2018.

[52] Jun Mei, Guancong Ma, Min Yang, Zhiyu Yang, Weijia Wen, and Ping Sheng. Dark acoustic metamaterials as super absorbers for low-frequency sound. *Nature Communications*, 3, 2012. ISSN 20411723. doi: 10.1038/ncomms1758.

[53] Koryo Miura. Method of Packaging and Deployment of Large Membranes in Space. *The institute of Space and Astronautical Science*, 618, 1985.

[54] Aditya Nanda and M.A. Karami. Tunable bandgaps in a deployable metamaterial. *Journal of Sound and Vibration*, 424:120–136, jun 2018. ISSN 0022-460X. doi: 10.1016/J.JSV.2018.03.015. URL https://www.sciencedirect.com/science/article/pii/S0022460X18301925.

[55] R. K. Narisetti, M. Ruzzene, and M. J. Leamy. A perturbation approach for analyzing dispersion and group velocities in two-dimensional nonlinear periodic lattices. *Journal of Vibration and Acoustics, Transactions of the ASME*, 133(6):1–12, 2011. ISSN 10489002. doi: 10.1115/1.4004661.

[56] Raj K. Narisetti, Michael J. Leamy, and Massimo Ruzzene. A perturbation approach for predicting wave propagation in one-dimensional nonlinear periodic structures. *Journal of Vibration and Acoustics, Transactions of the ASME*, 132(3):0310011–03100111, 2010. ISSN 10489002. doi: 10.1115/1.4000775.

[57] Raj K. Narisetti, Massimo Ruzzene, and Michael J. Leamy. Study of wave propagation in strongly nonlinear periodic lattices using a harmonic balance approach. *Wave Motion*, 49(2):394–410, 2012. ISSN 01652125. doi: 10.1016/j.wavemoti.2011.12.005. URL http://dx.doi.org/10.1016/j.wavemoti.2011.12.005.

[58] Antonio Palermo and Alessandro Marzani. Extended bloch mode synthesis: Ultrafast method for the computation of complex band structures in phononic media. *International Journal of Solids and Structures*, 100-101:29–40, 2016. ISSN 00207683. doi: 10.1016/j.ijsolstr.2016.06.033.

[59] M. Peeters, R. Viguié, G. Sérandour, G. Kerschen, and J. C. Golinval. Nonlinear normal modes, Part II: Toward a practical computation using numerical continuation techniques. *Mechanical Systems and Signal Processing*, 23(1):195–216, 2009. ISSN 08883270. doi: 10.1016/j.ymssp.2008.04.003.

[60] J. B. Pendry. Negative refraction makes a perfect lens. *Physical Review Letters*, 85(18):3966–3969, 2000. ISSN 00319007. doi: 10.1103/PhysRevLett.85.3966.

[61] Yan Pennec, Jérôme O. Vasseur, Bahram Djafari-Rouhani, Leonard Dobrzyński, and Pierre A. Deymier. Two-dimensional phononic crystals: Examples and applications. *Surface Science Reports*, 65(8):229–291, 2010. ISSN 01675729. doi: 10.1016/j.surfrep.2010.08.002. URL http://dx.doi.org/10.1016/j.surfrep.2010.08.002.

[62] Edwin A. Peraza-Hernandez, Darren J. Hartl, Richard J. Malak, and Dimitris C. Lagoudas. Origami-inspired active structures: A synthesis and review. *Smart Materials and Structures*, 23(9), 2014. ISSN 1361665X. doi: 10.1088/0964-1726/23/9/094001.

[63] A Srikantha Phani, J Woodhouse, and N Fleck. Wave propagation in two-dimensional periodic lattices. *Journal of the Acoustical Society of America*, 119(4):1995–2005, 2006.

[64] Phanisri P Pratapa, Phanish Suryanarayana, and Glaucio H Paulino. Design of Miura-Ori Patterns With Acoustic Bandgaps. In *Proceedings of the ASME 2017 International Design Engineering Technical Conferences and Computers and Information in Engineering Conference*, aug 2017. ISBN 978-0-7918-5818-9. doi: 10.1115/DETC2017-67384. URL https://doi.org/10.1115/DETC2017-67384.

[65] Phanisri P. Pratapa, Phanish Suryanarayana, and Glaucio H. Paulino. Bloch wave framework for structures with nonlocal interactions: Application to the design of origami acoustic metamaterials. *Journal of the Mechanics and Physics of Solids*, 118:115–132, 2018. ISSN 00225096. doi: 10.1016/j.jmps.2018.05.012.

[66] Min Qiu and Sailing He. A nonorthogonal finite-difference time-domain method for computing the band structure of a two-dimensional photonic crystal with dielectric and metallic inclusions. *Journal of Applied Physics*, 87(12):8268–8275, jun 2000. ISSN 0021-8979. doi: 10.1063/1.373537. URL http://aip.scitation.org/doi/10.1063/1.373537.

[67] V. Romero-García, J. V. Sánchez-Pérez, S. Castineira-Ibánez, and L. M. Garcia-Raffi. Evidences of evanescent Bloch waves in phononic crystals. *Applied Physics Letters*, 96(12), 2010. ISSN 00036951. doi: 10.1063/1.3367739.

[68] V. Romero-García, J. O. Vasseur, L. M. Garcia-Raffi, and A. C. Hladky-Hennion. Theoretical and experimental evidence of level repulsion states and evanescent modes in sonic crystal stubbed waveguides. *New Journal of Physics*, 14, 2012. ISSN 13672630. doi: 10.1088/1367-2630/14/2/023049.

[69] C. Rubio, D. Caballero, J. V. Sánchez-Pérez, R. Martínez-Sala, J. Sánchez-Dehesa, F. Meseguer, and F. Cervera. Existence of full gaps and deaf bands in two-dimensional sonic crystals. *Journal of Lightwave Technology*, 17(11):2202–2207, 1999. ISSN 07338724. doi: 10.1109/50.803012.

[70] Mark Schenk and Simon D. Guest. Origami Folding: A Structural Engineering Approach. In *Origami 5: Fifth International Meeting of Origami Science, Mathematics, and Education*, pages 291–304, Boca Raton, 2011. CRC Press.

[71] Mark Schenk and Simon D. Guest. Geometry of Miura-folded metamaterials. *Proceedings of the National Academy of Sciences of the United States of America*, 110(9):3276–3281, 2013. ISSN 00278424. doi: 10.1073/pnas.1217998110.

[72] C. Schröder. URV decomposition based structured methods for palindromic and even eigenvalue problems. 2007. URL http://opus4.kobv.de/opus4-matheon/frontdoor/index/index/docId/380.

[73] Christian Schröder. a Qr-Like Algorithm for the Palindromic Eigenvalue Problem. *Preprint*, 388:1–26, 2007.

[74] Wahyu Setyawan and Stefano Curtarolo. High-throughput electronic band structure calculations: Challenges and tools. *Computational Materials Science*, 49(2):299–312, aug 2010. ISSN 0927-0256. doi: 10.1016/J.COMMATSCI.2010.05.010. URL https://www.sciencedirect.com/science/article/pii/S0927025610002697?via{%}3Dihub.

[75] J. Shao, G. Liu, and L. Zhou. Biomimetic nanocoatings for structural coloration of textiles. *Active Coatings for Smart Textiles*, pages 269–299, jan 2016. doi: 10.1016/B978-0-08-100263-6.00012-5. URL https://www.sciencedirect.com/science/article/pii/B9780081002636000125.

[76] M M Sigalas and E N Economou. Attenuation of multiple-scattered sound. *Europhysics Letters*, 36(4):241–246, nov 1996. doi: 10.1209/epl/i1996-00216-4. URL https://doi.org/10.1209{%}2Fepl{%}2Fi1996-00216-4.

[77] Jesse L Silverberg, Arthur A Evans, Lauren Mcleod, Ryan C Hayward, Thomas Hull, Christian D Santangelo, and Itai Cohen. Using origami design principles to fold reprogrammable mechanical metamaterials. *Science*, 345(6197):647–650, 2014. URL `http://science.sciencemag.org/`.

[78] C. M. Soukoulis. *Photonic Crystals and Light Localization in the 21st Century*. Springer Netherlands, 1 edition, 2001. ISBN 978-0-7923-6948-6. doi: 10.1007/978-94-010-0738-2.

[79] Ian Stewart. Some assembly needed. *Nature*, 448:419, 2007. URL `http://internetconferences.net/ipsi/conference.`

[80] James Utama Surjadi, Libo Gao, Huifeng Du, Xiang Li, Xiang Xiong, Nicholas Xuanlai Fang, and Yang Lu. Mechanical Metamaterials and Their Engineering Applications. *Advanced Engineering Materials*, 21(3):1–37, 2019. ISSN 15272648. doi: 10.1002/adem.201800864.

[81] Tomohiro Tachi. Origamizing polyhedral surfaces. *IEEE Transactions on Visualization and Computer Graphics*, 16(2):298–311, mar 2010. ISSN 10772626. doi: 10.1109/TVCG.2009.67.

[82] Y. Tanaka, Y. Tomoyasu, and S. I. Tamura. Band structure of acoustic waves in phononic lattices: Two-dimensional composites with large acoustic mismatch. *Physical Review B - Condensed Matter and Materials Physics*, 62(11):7387–7392, 2000. ISSN 01631829. doi: 10.1103/PhysRevB.62.7387.

[83] Amir Ali Tavallaee and Jon P. Webb. Finite-element modeling of evanescent modes in the stopband of periodic structures. *IEEE Transactions on Magnetics*, 44(6):1358–1361, 2008. ISSN 00189464. doi: 10.1109/TMAG.2007.916490.

[84] M Thota. Origami Metastructures for Tunable Wave Propagation. In *Proceedings of the ASME 2016 Conference on Smart Materials, Adaptive Structures and Intelligent Systems*, Stowe, 2016.

[85] M. Thota and K. W. Wang. Reconfigurable origami sonic barriers with tunable bandgaps for traffic noise mitigation. *Journal of Applied Physics*, 122(15), oct 2017. ISSN 10897550. doi: 10.1063/1.4991026.

[86] M. Thota and K. W. Wang. Tunable waveguiding in origami phononic structures. *Journal of Sound and Vibration*, 430:93–100, sep 2018. ISSN 10958568. doi: 10.1016/j.jsv.2018.05.031.

[87] M Thota, S Li, and K W Wang. Lattice reconfiguration and phononic band-gap adaptation via origami folding. *Physical Review B*, 95:64307, 2017. doi: 10.1103/PhysRevB.95.064307.

[88] G. Trainiti, J. J. Rimoli, and M. Ruzzene. Wave propagation in periodically undulated beams and plates. *International Journal of Solids and Structures*, 75-76:260–276, 2015. ISSN 00207683. doi: 10.1016/j.ijsolstr.2015.08.019.

[89] Nicholas Turner, Bill Goodwine, and Mihir Sen. A review of origami applications in mechanical engineering. *Proceedings of the Institution of Mechanical Engineers, Part C: Journal of Mechanical Engineering Science*, 230(14):2345–2362, aug 2016. ISSN 20412983. doi: 10.1177/0954406215597713.

[90] Istvan A. Veres and Thomas Berer. Complexity of band structures: Semi-analytical finite element analysis of one-dimensional surface phononic crystals. *Physical Review B - Condensed Matter and Materials Physics*, 86(10):1–10, 2012. ISSN 10980121. doi: 10.1103/PhysRevB.86.104304.

[91] Istvan A. Veres, Thomas Berer, and Osamu Matsuda. Complex band structures of two dimensional phononic crystals: Analysis by the finite element method. *Journal of Applied Physics*, 114(8), 2013. ISSN 00218979. doi: 10.1063/1.4819209.

[92] V. G. Veselago. Te electrodynamics of substances with simultaneously negative values of ϵ and μ. *Soviet Physics Uspekhi*, 10(4):509–514, 1968.

[93] Eric King wah Chu, Tsung Ming Huang, Wen Wei Lin, and Chin Tien Wu. Palindromic eigenvalue problems: A brief survey. *Taiwanese Journal of Mathematics*, 14(3 A):743–779, 2010. ISSN 10275487. doi: 10.11650/twjm/1500405865.

[94] Scott Waitukaitis, Rémi Menaut, Bryan Gin Ge Chen, and Martin Van Hecke. Origami multistability: From single vertices to metasheets. *Physical Review Letters*, 114(5):2–6, 2015. ISSN 10797114. doi: 10.1103/PhysRevLett.114.055503.

[95] Yan Feng Wang, Yi Ze Wang, Bin Wu, Weiqiu Chen, and Yue Sheng Wang. Tunable and Active Phononic Crystals and Metamaterials. *Applied Mechanics Reviews*, 72(4), 2020. ISSN 00036900. doi: 10.1115/1.4046222.

[96] Yize Wang, Fengming Li, Yuesheng Wang, Kikuo Kishimoto, and Wenhu Huang. Tuning of band gaps for a two-dimensional piezoelectric phononic crystal with a rectangular lattice. *Acta Mechanica Sinica*, 25(1):65–71, feb 2009. ISSN 1614-3116. doi: 10.1007/s10409-008-0191-9. URL https://doi.org/10.1007/s10409-008-0191-9.

[97] Z. Y. Wei, Z. V. Guo, L. Dudte, H. Y. Liang, and L. Mahadevan. Geometric mechanics of periodic pleated origami. *Physical Review Letters*, 110(21):1–5, 2013. ISSN 00319007. doi: 10.1103/PhysRevLett.110.215501.

[98] Jihong Wen, Gang Wang, Dianlong Yu, Honggang Zhao, and Yaozong Liu. Theoretical and experimental investigation of flexural wave propagation in straight beams with periodic structures: Application to a vibration isolation structure. *Journal of Applied Physics*, 97(11), 2005. ISSN 00218979. doi: 10.1063/1.1922068.

[99] Tsung-Tsong Wu, Zi-Gui Huang, and S Lin. Surface and bulk acoustic waves in two-dimensional phononic crystal consisting of materials with general anisotropy. *Physical Review B*, 69(9):94301, 2004. doi: 10.1103/PhysRevB.69.094301. URL https://link.aps.org/doi/10.1103/PhysRevB.69.094301.

[100] Hong Jun Xiang and Zhi Fei Shi. Analysis of flexural vibration band gaps in periodic beams using differential quadrature method. *Computers and Structures*, 87(23-24):1559–1566, 2009. ISSN 00457949. doi: 10.1016/j.compstruc.2009.07.009. URL http://dx.doi.org/10.1016/j.compstruc.2009.07.009.

[101] Jie Yao, Zhaowei Liu, Yongmin Liu, Yuan Wang, Cheng Sun, Guy Bartal, Angelica M Stacy, and Xiang Zhang. Optical Negative Refraction in Bulk Metamaterials of Nanowires. *Science*, 321(5891):930, 2008. doi: 10.1126/science.1125907. URL http://science.sciencemag.org/content/321/5891/930.

[102] H. Yasuda, C. Chong, E. G. Charalampidis, P. G. Kevrekidis, and J. Yang. Formation of rarefaction waves in origami-based metamaterials. *Physical Review E*, 93(4):1–11, apr 2016. ISSN 24700053. doi: 10.1103/PhysRevE.93.043004.

[103] Hiromi Yasuda. *Wave dynamics in origami-based mechanical metamaterials*. 2018.

[104] Hiromi Yasuda and Jinkyu Yang. Tunable frequency band structures of origami-based mechanical metamaterials. *Journal of the international association for shell and spatial structures*, 58(4):287–294, 2017.

[105] Guilian Yi and Byeng D. Youn. A comprehensive survey on topology optimization of phononic crystals. *Structural and Multidisciplinary Optimization*, 54(5):1315–1344, 2016. ISSN 16151488. doi: 10.1007/s00158-016-1520-4. URL http://dx.doi.org/10.1007/s00158-016-1520-4.

[106] Dianlong Yu, Yaozong Liu, Honggang Zhao, Gang Wang, and Jing Qiu. Flexural vibration band gaps in Euler-Bernoulli beams with locally resonant structures with two degrees of freedom. *Physical Review B - Condensed Matter and Materials Physics*, 73(6):1–5, 2006. ISSN 10980121. doi: 10.1103/PhysRevB.73.064301.

[107] Dianlong Yu, Jihong Wen, Honggang Zhao, Yaozong Liu, and Xisen Wen. Vibration reduction by using the idea of phononic crystals in a pipe-conveying fluid. *Journal of Sound and Vibration*, 318(1-2):193–205, 2008. ISSN 0022460X. doi: 10.1016/j.jsv.2008.04.009.

[108] Jifeng Zhao, Ying Li, and Wing Kam Liu. Predicting band structure of 3D mechanical metamaterials with complex geometry via XFEM. *Computational Mechanics*, 55(4):659–672, 2015. doi: 10.1007/s00466-015-1129-2.

[109] W.X. Zhong and F.W. Williams. on the Direct Solution of Wave Propagation for Repetitive Structures. *Journal of Sound and Vibration*, 181(3):485–501, 1995.

[110] Xiang Zhou, Shixi Zang, and Zhong You. Origami mechanical metamaterials based on the Miura-derivative fold patterns. *Proceedings of the Royal Society A: Mathematical, Physical and Engineering Sciences*, 472, jul 2016. ISSN 14712946. doi: 10.1098/rspa.2016.0361.

A

Nonlinear band structures

The most commonly studied type of nonlinear phononic cystals are the granular phononic crystals (GPC) [14, 25, 57], in which the wave speed could be significantly tuned by applying a varying preload. Also, the wave speed could be tuned by varying the amplitude of the wave. The amplitude-dependent dispersion behaviour may also be found in (folded) plates, as thin-walled structures are prone to large geometrically nonlinear deformations.

Perturbation techniques–for instance the method of multiple scales–are commonly used in (weakly) nonlinear phononic crystals [25, 55, 56] to approximate the influence of nonlinearities on the dispersion relation. Alternatively, an harmonic balance approach [57] could be used, which can also be used for strongly nonlinear periodic lattices.

For nonlinear modal analysis problems, there exist several numerical methods to calculate the nonlinear normal modes (NNM) and their corresponding oscillation frequency. The two main methods are the shooting method and the pseudo-arclength continuation method [59], which both solve the equations of motion of the system in time domain.

Assuming that the geometric nonlinearities of the structure results in small additional forces, we can modify the equations of motions as:

$$\boldsymbol{M}\ddot{\boldsymbol{U}} + \boldsymbol{K}(\boldsymbol{k})\boldsymbol{U} = \epsilon \boldsymbol{f}_{NL}. \tag{A.1}$$

And using the dimensionless time:

$$\omega^2 \boldsymbol{M}\frac{\partial^2 \boldsymbol{U}}{\partial \tau^2} + \boldsymbol{K}(\boldsymbol{k})\boldsymbol{U} = \epsilon \boldsymbol{f}_{NL}, \tag{A.2}$$

where $|\epsilon| << 1$ is a small parameter quantifying the magnitude of the nonlinearity [50]. We then expand the eigenfrequency and the nodal displacement vectors

$$\begin{aligned} \omega &= \omega_0 + \epsilon\omega_1 + \mathcal{O}\left(\epsilon^2\right) \\ \boldsymbol{U} &= \boldsymbol{U}^{(0)} + \epsilon\boldsymbol{U}^{(1)} + \mathcal{O}\left(\epsilon^2\right) \end{aligned} \tag{A.3}$$

Substitution in Eq. (A.2), grouping by the order of ϵ and neglecting higher order terms

$$\mathcal{O}\left(\epsilon^0\right): \qquad \omega_0^2 \boldsymbol{M}\frac{\partial^2 \boldsymbol{U}^{(0)}}{\partial \tau^2} + \boldsymbol{K}(\boldsymbol{k})\boldsymbol{U}^{(0)} = \boldsymbol{0} \tag{A.4a}$$

$$\mathcal{O}\left(\epsilon^1\right): \qquad \omega_0^2 \boldsymbol{M}\frac{\partial^2 \boldsymbol{U}^{(1)}}{\partial \tau^2} + \boldsymbol{K}(\boldsymbol{k})\boldsymbol{U}^{(1)} = -2\omega_0\omega_1 \boldsymbol{M}\frac{\partial^2 \boldsymbol{U}^{(0)}}{\partial \tau^2} + \boldsymbol{f}_{NL}(\boldsymbol{U}^{(0)}) \tag{A.4b}$$

The first equation is the same as for the linear case, which can be solved using the same steps as above described. This solution can then be used to correct for the nonlinear parts. The second equation can by approximated by expanding the nonlinear force vector $\boldsymbol{f}_{NL}(\boldsymbol{U}^{(0)})$ in a Fourier series

$$\boldsymbol{f}_{NL} = \sum_{n=-\infty}^{+\infty} \boldsymbol{c}_n e^{in\tau}, \tag{A.5}$$

where

$$\boldsymbol{c}_n, j = \frac{1}{2\pi}\int_0^{2\pi} \boldsymbol{f}_{NL} e^{-in\tau} \mathrm{d}\tau, \tag{A.6}$$

and keeping only the $\boldsymbol{c}_1$ terms [50]. The eigenfrequencies of the $\mathcal{O}(\epsilon^1)$ system are the same as for the 0-th order system, the corresponding eigenmodes $\boldsymbol{\phi}_j$ are therefore also equal to the first order system. The $\mathcal{O}(\epsilon^1)$ system can then simply be soved for the frequency correction term ω_1, which is given by [50]

$$\omega_{1,j}(\boldsymbol{k}) = -\frac{\boldsymbol{\phi}_j^H(\boldsymbol{k})\boldsymbol{c}_1}{\omega_{0,j}|A|\boldsymbol{\phi}_j^H(\boldsymbol{k})\boldsymbol{M}\boldsymbol{\phi}_j(\boldsymbol{k})} \tag{A.7}$$

.

The tangent stiffness matrix of a geometric nonlinear shell can be written as combination of the linear stiffness matrix $\boldsymbol{K}$ and a geometric stiffness matrix $\boldsymbol{G}(\boldsymbol{U})$ [51]

$$\boldsymbol{K}_t(\boldsymbol{U}) = \boldsymbol{K} + \boldsymbol{G}(\boldsymbol{U}) \tag{A.8}$$

.

Substitution of Eq. (A.8) into Eq. (A.2), gives an expression for the nonlinear force

$$\boldsymbol{f}_{NL}(\boldsymbol{U}^{(0)}) = -\frac{1}{\epsilon}\boldsymbol{G}(\boldsymbol{U}^{(0)})\boldsymbol{U}^{(0)} \tag{A.9}$$

Using the definition of the Fourier series and using the assumed solution for $\boldsymbol{U}_0$, the first Fourier coefficient is obtained as:

$$\boldsymbol{c}_1 = -\frac{1}{\epsilon}\frac{A\boldsymbol{\phi}_j}{4\pi}\int_0^{2\pi}\boldsymbol{G}(\boldsymbol{U}^{(0)})\mathrm{d}\tau \tag{A.10}$$

There are however some technical issues when there are repeated eigenvalues. In those cases, the eigenmodes $\boldsymbol{\phi}_j$ are not uniquely defined as any linear combination of the eigenvectors is also a valid solution. However, the vector $\boldsymbol{c}_1$ depends on the eigenvectors in a nonlinear way, and the value will thus depend on the chosen combination of eigenvectors.

B

2D Representations complex band structures

This appendix contains 2D representations of the band structures from Figs. 2.4 and 2.7, which are shown in Figs. B.1 and B.2. For clarity, the imaginary components have been divided into four groups, which are based on the position of the real components on the IBZ. For instance, the $\Gamma - X$ graph shows all imaginary components for $\boldsymbol{k} \in [\Gamma, X)$, which are all wave vectors with real components on the $\Gamma - X$ path but not including X.

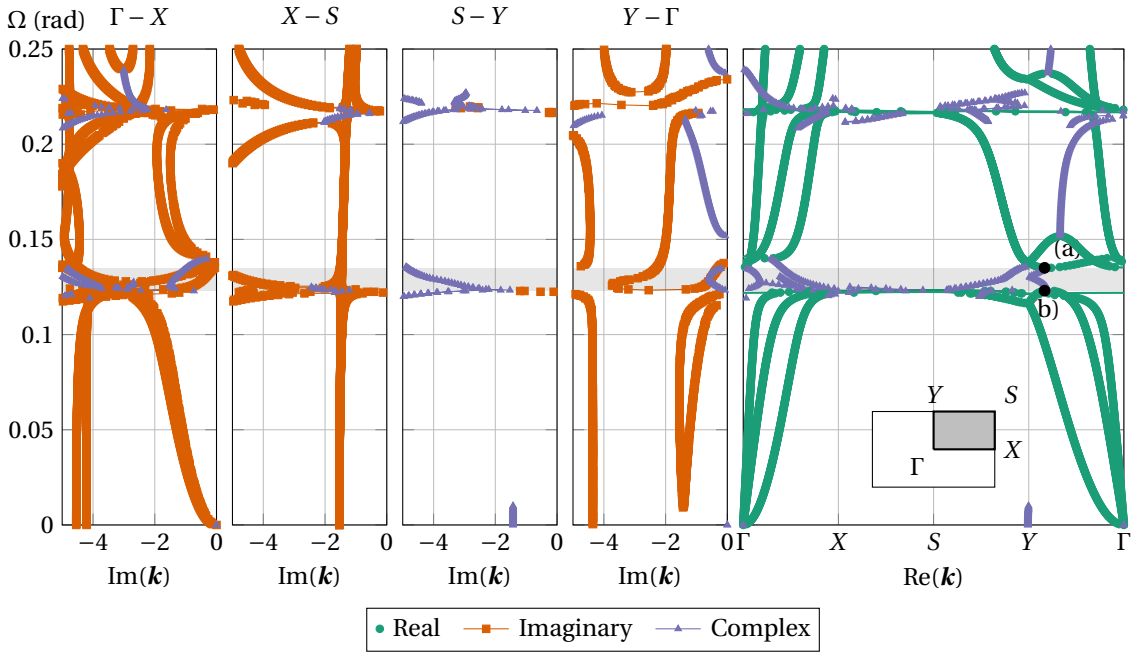

Figure B.1: The real and imaginary parts of the dispersion relation of the optimized Miura-Ori structure (optimum A).

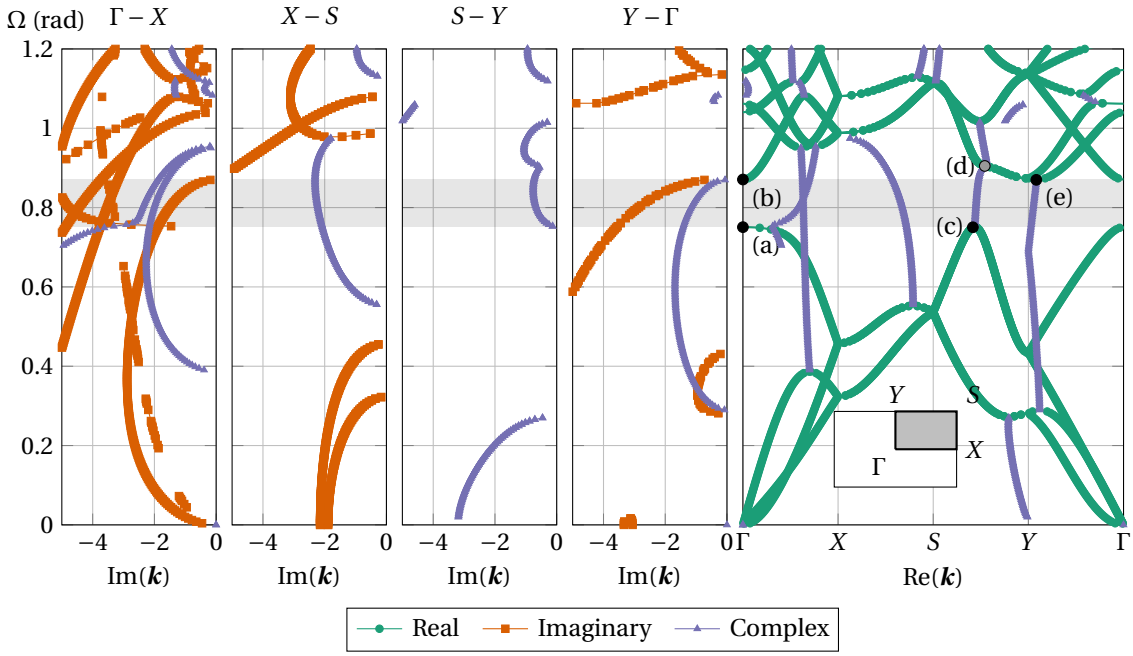

Figure B.2: A 2D representation of the real and imaginary parts of the dispersion relation of the optimized Miura-Ori structure for optimum B.